Response to Report #3 (Reviewer #3)

Thank you for reviewing our manuscript. Our response to the reviewer's comments and the corresponding text from the manuscript are presented below in blue and green fonts, respectively.

Reviewer's comment: The paper by Sakai et al. describes the setup of a trailer with a UV Raman lidar for water vapor measurements. This paper is a useful reference for future research with this system's data and data assimilation. The authors want to use the system for heavy rain forecasting. However, I still agree with reviewer two. This paper is not about heavy rain forecasting with a Raman lidar, as the title still suggests. And therefore I would still recommend to drop this part from the title. Maybe you can find an acronym for the lidar system name, that includes ". for heavy rain forecasting". And that acronym/name can be mentioned in the title. Overall, I would recommend the paper for publication, but I have some minor comments:

Our response:

From the Reviewers' comments, we realized that the real scope of this paper is to introduce the new compact mobile Raman lidar system, not about the heavy rain forecasting. Therefore, in accordance with the Reviewer's suggestions, we have changed the title of the manuscript from:

"Mobile water vapor Raman lidar for heavy rain forecasting: system instrument description and validation by comparison with radiosonde, GNSS, and high-resolution objective analysis"

to

"Automated compact mobile Raman lidar for water vapor measurement: instrument description and validation by comparison with radiosonde, GNSS, and high-resolution objective analysis".

Please find our point-to-point response to the Reviewer's comments below.

Reviewer comment:

1) The general problem, when the data shall be used for short-time forecasts of heavy rain events, is probably the occurrence of clouds. Whenever the water-vapor content is critically large, there are also low clouds, which in turn prohibit optimal lidar measurements. Therefore many people use synergistic approaches with different measurement systems (such as lidar, microwave radiometer, radar, GPS, ...) for such a task. This fact should be mentioned. Lidar is an important tool but not the only required instrument here.

Our response:

I agree with the Reviewer's comments that the lidar is unable to measure the water vapor distribution above the optically-thick clouds and thus it is important to use synergistic approaches with different measurement systems to measure the spatial and temporal distribution of the water vapor regardless of cloud occurrence. To mention this, we have added the following sentence (P16, L17-20):

"Despite the potential usefulness of the MRL-measured data for the weather forecasting, the MRL cannot measure the water vapor inside and above optically thick clouds. To overcome this disadvantage, it is important to use synergistic approaches with different instruments

such as GNSS, microwave radiometer, radiosonde to measure the water vapor distribution even under cloudy conditions (e.g., Foth and Pospichal, 2017)."

Reviewer comment:
2) Table 1: This table could be skipped and the few requirements written in one sentence. There are also no proper citations for these requirements, where do they come from?
Our response:
These requirements came from our discussion with the scientists involved in model development and implementation in our Institute. In accordance with the Reviewer's suggestion, we have deleted Table 1 and modified the sentences on the requirement in the Introduction as following (P1, L34-36):

"Given the temporal and vertical resolutions of the model and the assimilation window length, the required measurement resolutions are at most 30 min in time and 200 m in vertical."

Reviewer comment:
3) Table 2: The given beam divergence is before or after beam expansion? Please specify.
Our response:
It is after the beam expander. To specify this, we have added a notation in Table 2.

Reviewer comment:
4) Figure 1: The two lines from Laser and PIN to the electronics, should be drawn below the receiver box. Right now one line is on top of the beam path which is a bit confusing.
Our response:
In accordance with the Reviewer's comment, we have moved the two lines from the laser and PIN to the electronics below the receiver box. In addition to this change, we have added the window and light baffle in Fig. 1 in response to the reviewer's comment 7.

Reviewer comment:
5) P4L2: "The temperature is maintained to 22-32 degree C." That sounds not very stable. Can you find a few words on the actual stability? It seems that with a field of view of 0.3 mrad temperature stability, and thus laser beam alignment, is very crucial. Do you have any details on that, how the temperature affects the overlap alignment? Do you have a camera to check the alignment?
Our response:
The range of the variability of the temperature (22 and 32 degree Celsius) is the minimum and maximum values for the 5 months during the experimental period. The variation of air temperature in a day was mostly within a range of ±2 ºC. We did not find any change in laser and the overlap alignments. To avoid confusion of the readers, we have modified the text as following (P3, L7-9):

"The temperature inside the trailer is maintained within a range of ±2ºC between 22 ºC and 32 ºC by an air conditioner. We did not find any change of the optical alignment of the transmitter and receiver with the change of the temperature."

Reviewer comment:
6) How is the fused silica window constructed? Do you transmit and receive through the same window? Are there problems (especially if the window is dirty) with detector overloading from the scattering of the laser beam?

Our response:
It was constructed by the Kiyohara Optics Inc. (http://www.koptic.co.jp/opt/eng/index.html). We have added the manufacture's name in the text (P3, L10). We transmitted and received the light through the same window. There have not been any problems with detector overloading from the scattering of the laser beam. This might be partly owing to the light baffle between the window and telescope (Please see the modified version of Fig.1) that prevented light scattered by the window from entering the telescope. The other reason for that is rainwater occasionally washed away the dust on the window.

Reviewer comment:
7) It is mentioned that the data acquisition is analog and photon counting. Do you have any comments on the gluing procedure, or do you only use p.c. data, do you want to present any figure that shows the raw signals?
Our response:
We glued the analog and photon counting data. To clarify, we have added a following sentence (P4, L5-7):

"The P_X (z) for each receiving channel was obtained by connecting the photon counting and analog data using a count rate range of 1–10 MHz (mostly 0.2–0.4 km for the water vapor and 0.5–0.9 km for the nitrogen channels) to gain high dynamic range."

Reviewer comment:
8) Fig 10, P8L39. A very narrow interference filter is used. Did you consider a temperature correction of the 407 nm signal with help of the filter's transmission curve? This might be the reason for the discrepancies above 5 km height. At least mention that the issue might be relevant here.
Our response:
We have evaluated the temperature variation of the effective Raman cross section (i.e. integrated Raman backscattering cross section multiplied by filter's transmission) using the filter's transmission curves provided from the manufacture and the Raman cross sections (Penny and Lapp, 1976; Inaba, 1976; Avila et al., 2014). We found that the variation is 0.5% for the temperature range of 253–303 K (Fig. A1). Thus, the issue is negligible for the reason for the discrepancy. We have added a following comment (P9, L1-3):

"The influence of the temperature dependence of the Raman cross section (e.g. Whiteman, 2003) is negligible for the MRL because the variation is estimated to be 0.5% for the temperature range of 253–303 K."

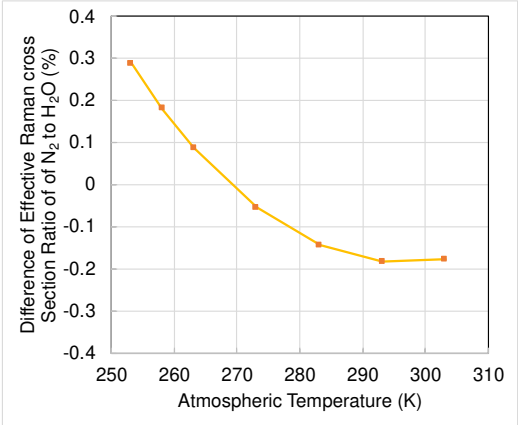

Figure A1. Temperature variation of difference of the ratio of effective Raman cross section of nitrogen to water vapor channels of MRL.

Reviewer comment:
9) Fig 11/13/14/ Table 3: When there is the calculation of the slope and intercept, I suggest to also give the statistical error of these values from the fit. Then you can determine if the slope difference from 1/unity is indeed significant or not.
Our response:
In accordance with the Reviewer's comment, we have added the statistical uncertainties of the slopes and intercepts of the regression analysis in the revised manuscript of Table 2 and the text (P11, L14-15). We note that the results of the regression analysis have been slightly changed because we have corrected the number of the data points by deleting the points that were mistakenly counted before.

Reviewer comment:
10) P14L17. The first sentence misses a dot.
Our response: Corrected.

Reviewer comment:
11) P17L3-5: This is a single sentence paragraph. I suggest connecting the sentence to the previous paragraph.
Our response: Corrected.

Reviewer comment:
12) I suggest harmonizing the figures for equal font size, line width, and resolution.
Our response:
In accordance with the suggestion, we have harmonized the figures for font size, line width and resolution as possible as we could.

Reviewer comment:
13) I realized that there are not many references within this manuscript, although many have been published on the topic of water vapor Raman lidars, calibration, and assimilation. Here are just a few that might be useful:

1. Dai, G., Althausen, D., Hofer, J., Engelmann, R., Seifert, P., Bühl, J., Mamouri, R.-E., Wu, S., and Ansmann, A.: Calibration of Raman lidar water vapor profiles by means of AERONET photometer observations and GDAS meteorological data, Atmos. Meas. Tech., 11, 2735-2748, https://doi.org/10.5194/amt-11-2735-2018, 2018.

2. Foth, A. and Pospichal, B.: Optimal estimation of water vapour profiles using a combination of Raman lidar and microwave radiometer, Atmos. Meas. Tech., 10, 3325-3344, https://doi.org/10.5194/amt-10-3325-2017, 2017.

3. Foth, A., Baars, H., Di Girolamo, P., and Pospichal, B.: Water vapour profiles from Raman lidar automatically calibrated by microwave radiometer data during HOPE, Atmos. Chem. Phys., 15, 7753-7763, https://doi.org/10.5194/acp-15-7753-2015, 2015.

4. Bhawar et. all 2011, The water vapour intercomparison effort in the framework of the Convective and Orographically induced Precipitation Study: airborne to ground based and airborne to airborne lidar systems

https://doi.org/10.1002/qj.697

5. Herold, C., D. Althausen, D. Müller, M. Tesche, P. Seifert, R. Engelmann, C. Flamant, R. Bhawar, and P. Di Girolamo, 2011: Comparison of Raman Lidar Observations of Water Vapor with COSMO-DE Forecasts during COPS 2007. Wea. Forecasting, 26, 1056–1066, https://doi.org/10.1175/2011WAF2222448.1

6. Grzeschik, Matthias & Bauer, Hans-Stefan & Wulfmeyer, Volker & Engelbart, Dirk & Wandinger, Ulla & Mattis, Ina & Althausen, Dietrich & Engelmann, Ronny & Tesche, Matthias & Riede, Andrea. (2008). Four-Dimensional Variational Data Analysis of Water Vapor Raman Lidar Data and Their Impact on Mesoscale Forecasts. Journal of Atmospheric and Oceanic Technology - J ATMOS OCEAN TECHNOL. 25. 10.1175/2007JTECHA974.1.

Our response:

Thank you for introducing the references that are useful for readers. We have added them in the manuscript (i.e. Ref. 1 in P5, L35; Ref. 2 in P16, L20; Refs. 4 and 5 in P7, L22, and Ref. 6 in P1, L32). In addition to these references, we have added the following references that are relevant for the topic of the manuscript.

On the validation of the Raman lidar (P7, L22):
Behrendt, A., V. Wulfmeyer, H. Bauer, T. Schaberl, P. Di Girolamo, D. Summa, C. Kiemle, G. Ehret, D.N. Whiteman, B.B. Demoz, E.V. Browell, S. Ismail, R. Ferrare, S. Kooi, and J. Wang: Intercomparison of Water Vapor Data Measured with Lidar during IHOP_2002. Part I: Airborne to Ground-Based Lidar Systems and Comparisons with Chilled-Mirror Hygrometer Radiosondes, J. Atmos. Oceanic Technol., 24, 3–21, https://doi.org/10.1175/JTECH1924.1, 2007.

On the data assimilation of the lidar data (P1, L32):
Bielli, S., Grzeschik, M. , Richard, E. , Flamant, C. , Champollion, C. , Kiemle, C. , Dorninger, M. and Brousseau, P.: Assimilation of water□vapour airborne lidar observations: impact study on the COPS precipitation forecasts, Q. J. R. Meteorol. Soc., 138: 1652-1667. doi:10.1002/qj.1864, 2012.

Wulfmeyer, V., H. Bauer, M. Grzeschik, A. Behrendt, F. Vandenberghe, E.V. Browell, S. Ismail, and R.A. Ferrare: Four-Dimensional Variational Assimilation of Water Vapor Differential Absorption Lidar Data: The First Case Study within IHOP_2002, Mon. Wea. Rev., 134, 209–230, https://doi.org/10.1175/MWR3070.1, 2006.

On the calibration of water vapor mixing ratio (P5, L35):
David, L., Bock, O., Thom, C., Bosser, P., and Pelon, J.: Study and mitigation of calibration factor instabilities in a water vapor Raman lidar, Atmos. Meas. Tech., 10, 2745-2758, https://doi.org/10.5194/amt-10-2745-2017, 2017.

In addition to these changes, we have added the following sentence in the Conclusion to clarify that the MRL can also be utilized for the study of water vapor in the lower troposphere (P19, L5-7):
“Although the MRL system was originally developed for heavy rain forecasting, it can also be utilized for the study of water vapor in the lower troposphere such as boundary layer structure and cloud formation.”

We mention that the sentences explaining the specification of the radiosonde and the local analysis data originally in Sec. 3 have been moved to Sec. 3.1 and 3.3, respectively, to be easy to read.

Thank you again for his or her valuable comments.

References:

Avila, G., J.M. Fernández, G. Tejeda, S. Montero: The Raman spectra and cross-sections of H2O, D2O, and HDO in the OH/OD stretching regions, J. Mol. Spectrosc., 228, 38-65, https://doi.org/10.1016/j.jms.2004.06.012, 2004.

Inaba, H.: Detection of atoms and molecules by Raman and resonance fluorescence, In Laser Monitoring of the Atmosphere, Springer-Verlag, pp.153–236, 1976.

Penney, C. M. and Lapp, M.: Raman-scattering cross sections for water vapor, J. Opt. Soc. Am., 66, 422–425, 1976.

Response to Report #1 (from Reviewer #2)

Thank you for reviewing our manuscript. Our response to the reviewer's comments and the corresponding text from the manuscript are presented below in blue and green fonts, respectively.

Reviewer's Comment: I reviewed the updated version of the manuscript by et Sakai et al. To accommodate the reviewer's requests, the authors spent mainly their effort in slightly changing the tone of the manuscript and to demonstrate to some extent that the system they are describing is related to the rain forecasting system, though smoothing the final goal which is clearer now but to my opinion not fully in line with the objective of AMT journal.

This is stated in home page of the journal and it is:

Atmospheric Measurement Techniques (AMT) is an international scientific journal dedicated to the publication and discussion of advances in remote sensing, as well as in situ and laboratory measurement techniques for the constituents and properties of the Earth's atmosphere.
The main subject areas comprise the development, intercomparison, and validation of measurement instruments and techniques of data processing and information retrieval for gases, aerosols, and clouds. Papers submitted to AMT must contain atmospheric measurements, laboratory measurements relevant for atmospheric science, and/or theoretical calculations of measurements simulations with detailed error analysis including instrument simulations.

So not only a description of a measurement systems or intercomparison are required but advances in measurement field must be reported
The authors state that to their knowledge, such a small mobile Raman lidar has only been reported by Chazette et al. (2015).

Reviewing the literature, the authors may easily find, for example, the following paper in addition to the one by Chazette et al.

Engelmann et al., "The automated multiwavelength Raman polarization and water-vapor lidar PollyXT: the neXT generation", Atmos. Meas. Tech., 9, 1767-1784, https://doi.org/10.5194/amt-9-1767-2016, 2016.

This paper describes the most recent version of a portable multi-wavelength Raman and polarization lidar PollyXT equipped with a water-vapor Raman channel.

In additional we may also consult the following link:

https://infoscience.epfl.ch/record/140620

https://www.raymetrics.com/product/temperature-and-humidity-lidar

Therefore, the system described by the authors is definitely not one of the first attempt to deploy a compact Raman lidar system able to operate on a continuous basis. About the Polly XT system's performances, they look similar to those described in the manuscript by Sakai et al., with a better full overlap height.

The authors also continue to state that the system description could be very beneficial for investigating measurement locations that are effective for the heavy rain forecasting. In literature there are other paper demonstrating the value of assimilating water vapour Raman lidar measurements in forecast models. Here, the authors refers to a paper by Yoshida et al. 2018, "Feasibility study of data assimilation using a mobile water vapor" which is a proceeding to conference of 4-pages, quite limited to fully demonstrate a big thesis like the impact of Raman lidar measurement on a forecasting system.

In the paper by Yoshida et al., the results collected over about two months-experiment are condensed in one example where there is a certain impact due to the Raman lidar data assimilation though this is not striking when the heavier rain fall comes. Nevertheless, it's not my role to judge the other paper but I think that for sure the paper does not show a large benefit in assimilating Raman lidar water vapor measurements up to 1.0-1.5 km during daytime. Though this may be theoretically useful, it must be demonstrated that the measurements of their system, close and within the incomplete overlap region are really useful and cannot impact negatively the forecasts.

To this purpose, the authors provide an estimation of the total uncertainty for the overlap correction of at most 23%, which is quite high in a region where the atmospheric variability requires a higher accuracy for the data to have an impact on the forecast model.

My opinion is that there is still limited interest in having another manuscript which mainly does not provide any special advance in the usage of the Raman lidar technique for measuring water vapour. The interest in the readers can only come from the fact that a new compact Raman lidar system for monitoring water vapour is available (also on the market?) and can be operated in a measurement network or at a remote station. The manuscript does not need to necessarily be linked to the scope of improving rainfall forecasting but to many other applications, like for any other Raman lidar system. The manuscript does not reveal any special feature of this lidar system which can significantly improve the weather forecasts with respect to other systems previously presented in literature.
Therefore, the manuscript must be necessarily reshaped to consider the real scope of this paper: to introduce another automated compact Raman lidar for water vapour measurements, which has an affordable cost (<250K US dollars) and apparently easy to be operated. I do not think this requires a strong effort but the manuscript will benefit from this work and may be of some interest to the community.
Under these premises, if the editor feels that this is line with the scope of the journal, I recommend major revisions and I am happy to further support the Editor in any following step of this review procedure.

Response:

We agree with the Reviewers' comment and realized that the real scope of this paper is to introduce the automated compact Raman lidar for water vapour measurements which has an affordable cost and easy to be operated, not necessarily to improve rainfall forecasting. Therefore, we have changed the title from:

"Mobile water vapor Raman lidar for heavy rain forecasting: system instrument description and validation by comparison with radiosonde, GNSS, and high-resolution objective analysis"

to

"Automated compact mobile Raman lidar for water vapor measurement: instrument description and validation by comparison with radiosonde, GNSS, and high-resolution objective analysis".

Further, to clarify the scope of the paper we have modified the Abstract and Conclusion. For example, we have changed the first sentence of the Abstract from (P1, L9-10):

"To improve the lead time and accuracy of predictions of localized heavy rainfall, which can cause extensive damage in urban areas in Japan, we developed a mobile Raman lidar (MRL) system for measuring the vertical distribution of the water vapor mixing ratio (w) in the lower troposphere."

to

"We developed an automated compact mobile Raman lidar (MRL) system for measuring the vertical distribution of the water vapor mixing ratio (w) in the lower troposphere which has an affordable cost and easy to be operated."

We have also changed the last sentence of the Abstract from (P1, L19-20):

"Four months of continuous operation of the MRL system demonstrated its utility for monitoring water vapor distributions for heavy rain forecasting."

to

"Four months of continuous operation of the MRL system demonstrated its utility for monitoring water vapor distributions in the lower troposphere."

Similarly, we have changed the first sentence in the Conclusion from (P16, L26-28):

"We developed a mobile Raman lidar system for measuring the vertical distribution of the water vapor mixing ratio w in the lower troposphere to improve the accuracy and lead time of heavy rainfall prediction."

to

"We developed a low-cost, automated compact mobile Raman lidar system for measuring the vertical distribution of the water vapor mixing ratio w in the lower troposphere, which is easy to be deployed to remote sites and is capable of unattended operation for several months."

And we have added the following sentence to clarify that the MRL can be utilized not only for rainfall forecasting but also the other study of the water vapor in the lower troposphere (P17, L5-6):

"Although the MRL system was originally developed for heavy rain forecasting, it can also be utilized for the study of water vapor in the lower troposphere."

In addition to these changes, we have revised the manuscript in accordance with the comments from the Reviewer #3. Please find the marked-up manuscript version showing the

changes we have made. We trust that the revised manuscript is in line with the scope of the journal.

Thank you again for his or her valuable comments.

Automated compact ~~Mobile~~ mobile ~~water vapor~~ Raman lidar for water vapor measurement ~~for heavy rain forecasting~~: instrument description and validation by comparison with radiosonde, GNSS, and high-resolution objective analysis

Tetsu Sakai[1], Tomohiro Nagai[1], Toshiharu Izumi[2], Satoru Yoshida[1], Yoshinori Shoji[1]

[1]Meteorological Satellite and Observation System Research Department, Meteorological Research Institute, Tsukuba, 305-0052 Ibaraki, Japan
[2]Observation Department, Japan Meteorological Agency, 1-3-4 Otemachi, Chiyoda-ku, 100-8122 Tokyo, Japan

Correspondence to: Tetsu Sakai (tetsu@mri-jma.go.jp)

Abstract. ~~To improve the lead time and accuracy of predictions of localized heavy rainfall, which can cause extensive damage in urban areas in Japan, w~~We developed an automated compact mobile Raman lidar (MRL) system for measuring the vertical distribution of the water vapor mixing ratio (w) in the lower troposphere which has an affordable cost and easy to be operated. The MRL was installed in a small trailer for easy deployment ~~to the upwind side of potential rainfall areas~~ and can start measurement in a few hours, and is capable of unattended operation for several months~~to monitor the inflow of moist air before rainfall events~~. We describe the MRL system and present validation results obtained by comparing the MRL-measured data with collocated radiosonde, Global Navigation Satellite System (GNSS), and high-resolution objective analysis data. The comparison results showed that MRL-derived w agreed within 10% (root-mean-square difference of 0.98 g/kg) with values obtained by radiosonde at altitude ranges between 0.14 and 1.5 km in the daytime and between 0.14 and 5–6 km at night in the absence of low clouds; the vertical resolution of the MRL measurements was 75−150 m, their temporal resolution was less than 20 min, and the measurement uncertainty was less than 30%. MRL-derived precipitable water vapor values were similar to or slightly lower than those obtained by GNSS at night, when the maximum height of MRL measurements exceeded 5 km. The MRL-derived w values were at most 1 g/kg (25%) larger than local analysis data. Four months of continuous operation of the MRL system demonstrated its utility for monitoring water vapor distributions ~~for heavy rain forecasting~~in the lower troposphere.

1 Introduction

In recent years, the occurrence frequency of localized heavy rainfall capable of causing extensive damage has been increasing in urban areas of Japan (Japan Meteorological Agency (JMA), 2016). For early prediction of heavy rainfall, a numerical weather prediction (NWP) model is employed along with conventional meteorological observation data. However, the lead time (period of time between the issuance of a forecast and the occurrence of the rainfall) and accuracy of the prediction are limited, in part, because of the coarse temporal and spatial resolutions of water vapor distribution observations. To improve those observations, we developed a low-cost, automated ~~-~~mobile Raman lidar (MRL) system that can continuously measure the vertical distribution of water vapor in the lower troposphere. The MRL can be easily deployed at a site upwind of a potential heavy rainfall area and start measurement in a few hours to monitor the vertical water vapor distribution before a rainfall event. As several studies have already demonstrated a strong and positive impact of the water vapor lidar data on the initial water vapor field of the numerical weather prediction mesoscale model by using the three- or four-~~-~~dimensional variational method (Wulfmeyer et al., 2006; Grzeschik et al., 2008; Bielli et al., 2011), the MRL-measured data can ~~then~~ be assimilated into a nonhydrostatic mesoscale model (NHM) (Saito et al., 2007) by the local ensemble transform Kalman filter (LETKF) method (Kunii, 2014) to improve the initial condition of the water vapor field and consequently the rainfall forecast. ~~We discussed~~

with scientists involved in model development and implementation the required temporal and spatial resolution and accuracy of the measured data for heavy rain forecastingGiven the temporal and vertical resolutions of the model and the assimilation window length, the required measurement resolutions are at most 30 min in time and 200 m in vertical. The measurement altitude range should be at least between 0.2 km and 2 km, becauseFor the measurement altitude range, Kato (2018) has reported that the equivalent potential temperature at a height of 500 m, which is a function of the water vapor concentration at that height, is an important parameter for forecasting heavy rainfall in the Japanese area because the inflow of moist air, which can cause heavy rain, mainly occurs at around that altitude. Thus, the measurable altitude range must extend upward to at least that altitude. The measurement uncertainty (observation error) should be less than 10% and must be specified. Wulfmeyer et al. (2015) discussed the requirements of accuracy of the lower tropospheric water vapor measurement for data assimilation and reported that it should be smaller than 10% in noise error and < 5% in bias error. Besides the requirement of measurement accuracy, reducing the cost of the lidar is important because it makes easier to distribute them around the forecasting area to increase the opportunity of detecting the inflow. We developed our mobile MRL system to meet these requirements as much as possible within the total material cost of ~250K USD. The Raman lidar technique is a well-established technique for measuring the water vapor distribution in the troposphere (e.g. Melfi et al., 1969, Whiteman et al., 1992), and the systems have been in operation for decades at stations around the world (Turner et al., 2016; Dinoev et al., 2013; Reichardt et al., 2012; Leblanc et al., 2012). Field-deployable systems have also been developed by several institutes (Whiteman et al., 2012; Chazette et al., 2014; Engelmann et al., 2016). Our MRL system is a compact mobile system that can be deployed on a standard vehicle and operated unattended for several months by remote control. To our knowledge, there are few reports on the validation for such a compact mobile system. As the first step of our goal aiming to develop the heavy rainfall forecasting system, here we describe our mobile lidar system and present validation results obtained by comparing the MRL-measured data with data obtained by other humidity sensors as well as objective analysis data. Section 2 of this paper describes the MRL instrumentation and the data analysis method. Section 3 presents the validation results obtained by comparing the MRL measurements with collocated radiosonde measurements, GNSS data, and high-resolution objective analysis data provided by the JMA. Section 4 is a summary.

Table 1. Lidar data requirements for localized heavy rain forecasting

System	Field deployable
Measured quantity	Water vapor mixing ratio (w)
Data description	
- Altitude range	<0.2 km to >2 km
- Time period	24-hour, continuous
- Vertical resolution	<200 m
- Temporal resolution	<30 min
- Uncertainty	<10%

2 Instrumentation

2.1 Transmitter and receiver optics

The MRL system employs a Nd:YAG laser (Continuum Surelite EX) operating at 355 nm with pulse energy of 200 mJ and a repetition rate of 10 Hz. The beam diameter is expanded fivefold to a diameter of ~5 cm by a beam expander (CVI, USA), and the beam is emitted vertically into the atmosphere. The light backscattered by atmospheric gases and particles is collected by

a custom-made Cassegrain telescope (primary mirror diameter of 0.35 m, focal length 3.1 m; Kyoei Co., Japan). The focal point of the telescope is within the tube to shorten the length of the receiving system. Light baffles placed inside the telescope tube prevent stray light from entering the detectors. The received light is separated into three spectral components, Raman water vapor (407.5 nm), nitrogen (386.7 nm), and elastic (355 nm) backscatter light, with dichroic beam splitters and interference filters (IFs) (Barr Materion, USA), shortcut filters (Isuzu Glass ITY385, Japan), and shortpass filters (SHPF-50S-440, SIGMAKOKI, Japan) and detected by photomultiplier tubes (PMTs) (R8619, Hamamatsu, Japan). The interference filter angles of the Raman channels are tuned manually to maximize the transmission of the Raman backscatter signal. To avoid signal saturation of the PMTs, we inserted neutral density filters before the PMTs. The signals are acquired with a transient recorder (Licel TR-20-160) operating in analog (12-bit) and photon counting (20 MHz) modes. The data are stored on the hard disk of a personal computer (PC). The MRL can be operated remotely by issuing commands (e.g. turn high voltage of PMTs on/off, start/stop lasing, start/stop data acquisition, and transfer data) to the PC via wireless Internet communication (Table ~~2~~1, Fig. 1).

Table ~~2~~1. Specifications of the mobile Raman lidar

Transmitter:			
Laser	Nd:YAG		
Wavelength (nm)	355		
Pulse energy (mJ)	220 (maximum)		
Repetition frequency (Hz)	10		
Beam divergence (mrad)	0.125 (after beam expander)		
Receiver:			
Telescope type	Cassegrain		
Diameter of primary mirror (m)	0.35		
Field of view (mrad)	0.29		
Detectors	Photomultiplier tubes		
Data acquisition	Photon counting/analog		
Detection specifications:	Raman water vapor	Raman nitrogen	Elastic
Interference Filter			
Center wavelength (nm)	407.65	386.65	354.63
Bandwidth (nm)	0.25	0.34	0.6
Peak transmission (%)	74	45	43
Rejection at 355 nm	$<10^{-13}$	$<10^{-7}$	–

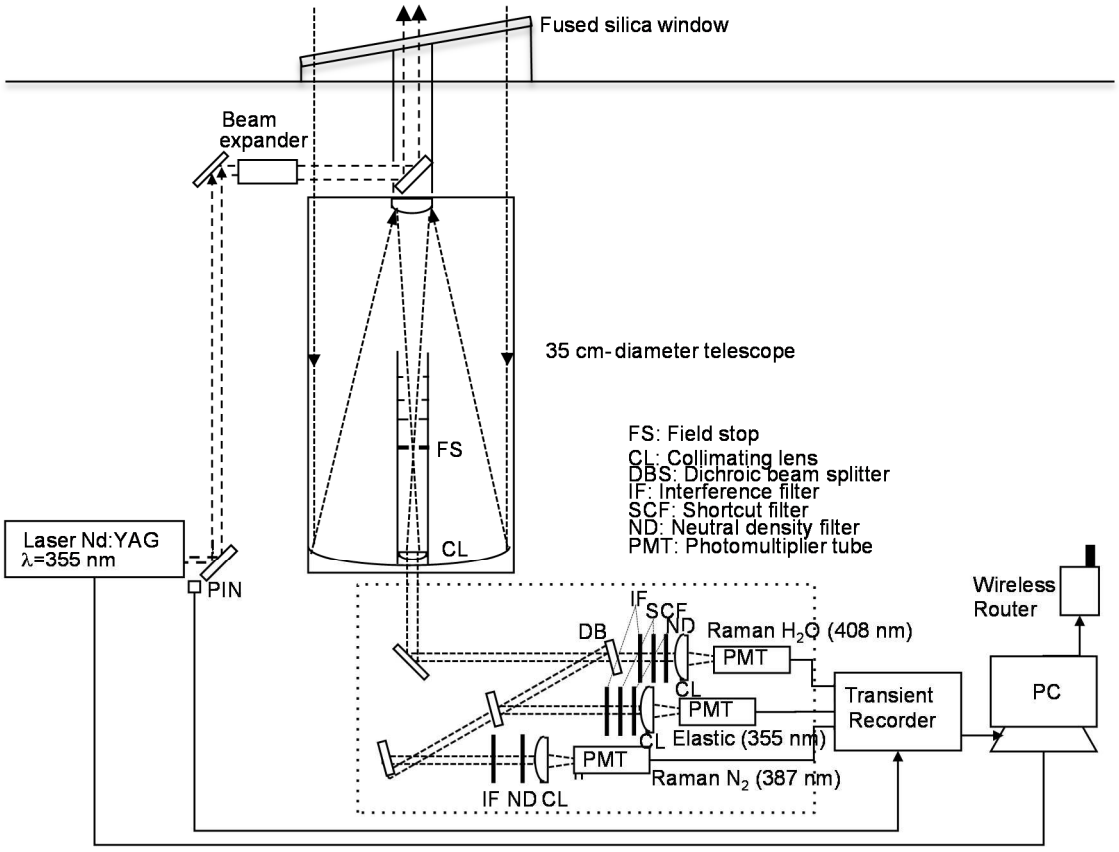

Figure 1. Schematic diagram of the mobile Raman lidar system.

2.2 Trailer

The MRL system is enclosed in a container with outside dimensions of 1.7 m by 4.2 m by 2.1 m high (Figs. 2 and 3). The total weight, including the lidar system and the trailer, is approximately 800 kg. The trailer can be towed behind any standard-sized vehicle; therefore, anyone who holds a basic-class driver's license can tow it in Japan. The temperature inside the trailer is maintained within a range of ±2ºC ~~to~~ between 22 ºC and~~–~~ 32 ºC by an air conditioner during the experimental period in 2016. We did not find any change of the optical alignment of the transmitter and receiver with the change of the temperature. A fused silica window (47 cm × 42 cm × 1 cm thick, Kiyohara Optics, Inc.) with an antireflection coating installed at a tilt angle of 10° above the receiving telescope enables the MRL to be operated regardless of the weather. To prevent direct sunlight from entering the telescope, a chimney-type light baffle with a height of 2 m is mounted on top of the trailer. The system requires a single-phase, three-wire type 100/200V power supply with a maximum current of 10A (5–7 A during normal operation).

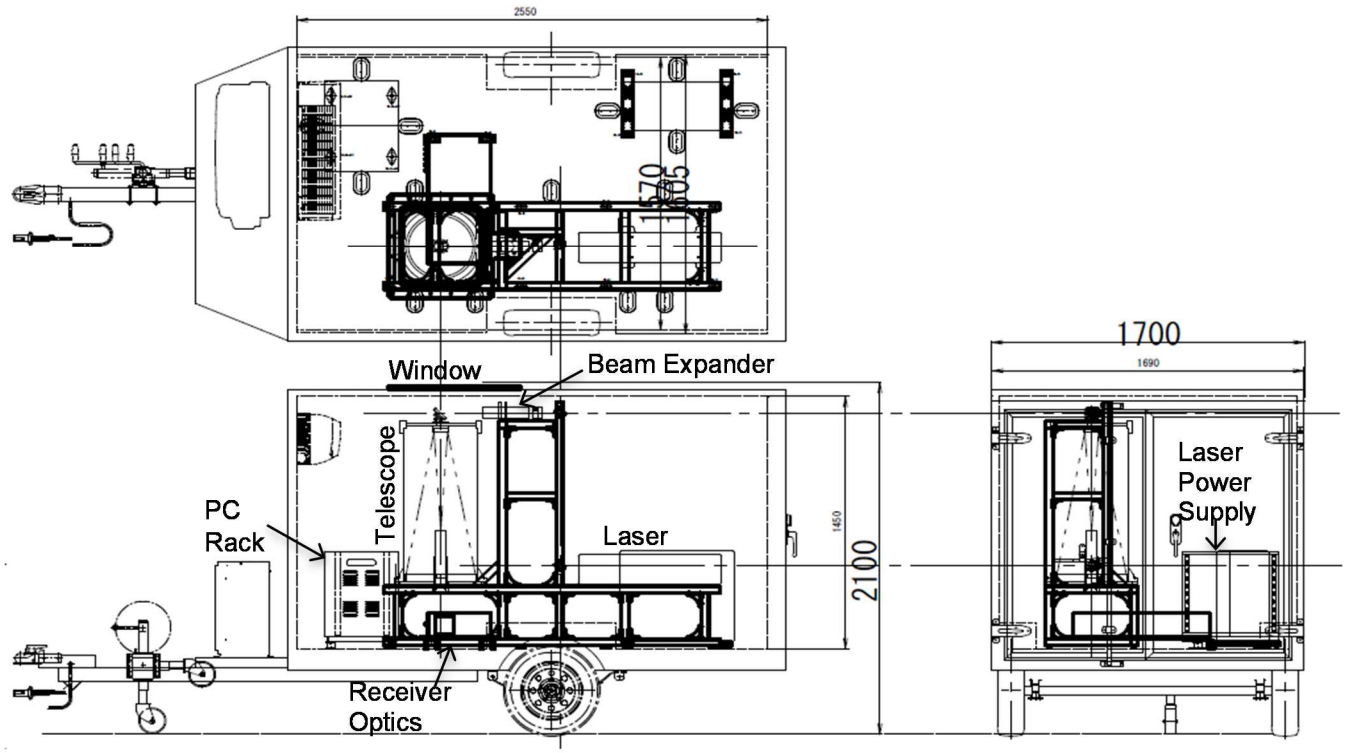

Figure 2. Layout of the mobile Raman lidar system in its trailer. Dimensions are in millimeters.

Figure 3. Photographs of the MRL trailer (left) and its interior (right).

2.3 Data analysis

The water vapor mixing ratio (w) is obtained from the observed Raman backscatter signal of water vapor and nitrogen as follows:

$$w(z) = K \frac{O_{H_2O}(z)}{O_{N_2}(z)} \frac{P_{H_2O}(z)}{P_{N_2}(z)} \Delta T(z_0, z),$$

with

$$\Delta T = \frac{e^{\int_{z_0}^{z} [\alpha_{H_2O}^{m}(z') + \alpha_{H_2O}^{p}(z')] dz'}}{e^{\int_{z_0}^{z} [\alpha_{N_2}^{m}(z') + \alpha_{N_2}^{p}(z')] dz'}}, \quad (1)$$

where K is the calibration coefficient of the water vapor mixing ratio, $O_X(z)$ is the beam overlap function of the receiver's channel, and $P_X(z)$ is the noise-subtracted Raman backscatter signal of molecular species X (H_2O or N_2) at height z from the lidar at z_0, ΔT is the transmission ratio of the Ramen signals between the lidar at z_0 and z, and α_X^m and α_X^p are the molecular and particle extinction coefficients of X at the wavelength of the Raman scattering. The $P_X(z)$ for each receiving channel was obtained by connecting the photon counting and analog data using a count rate range of 1–10 MHz (mostly 0.2–0.4 km for the water vapor and 0.5–0.9 km for the nitrogen channels) to gain high dynamic range. The value of K was obtained by comparing the uncalibrated MRL-derived value of w (i.e. w computed assuming $K = 1$ in Eq. 1) with w obtained with a radiosonde launched 80 m northeast of the MRL at 20:30 LST by a weighted least squares method (Sakai et al., 2007) between altitudes of 1 and 5 km and taking the average over the measurement period. See Sect. 2.4 for the values of K obtained in this manner and their temporal variation. In this system, the ratio of the beam overlap functions ($\frac{O_{H_2O}(z)}{O_{N_2}(z)}$) is 1 above an altitude of 0.5 km, and below that altitude it deviates slightly from 1; these values were determined by comparing the MRL-derived value of w without overlap correction (i.e. w obtained by assuming $\frac{O_{H_2O}(z)}{O_{N_2}(z)} = 1$ in Eq. 1) with w obtained by radiosonde measurements (see Sect. 2.5). To determine ΔT, we calculated α_X^m using molecular extinction cross section (Bucholz, 1995) atmospheric density obtained from the radiosonde measurement made closest to the MRL measurement period; we did not take the differential aerosol extinction for the two Raman wavelengths into account because it is usually less than 5% below the altitude of 7 km (i.e. ΔT ranges from 1 to 0.95 from the lidar position to 7 km) under normal aerosol loading conditions (Whiteman et al., 1992). The temporal and vertical resolutions of the raw data were 1 min and 7.5 m, respectively. To reduce the statistical uncertainty of the derived w, we averaged the raw data over 20 min and reduced the vertical resolution to 75 m below 1 km altitude and 150 m above that. The measurement uncertainty of w was estimated from the photon counts by assuming Poisson statistics (e.g. Whiteman, 2003) and the uncertainty of the calibration coefficient as follows:

$$\delta w(z) = \left[\left(\frac{\delta K}{K}\right)^2 + \left(\frac{\delta P_{H_2O}(z)}{P_{H_2O}(z)}\right)^2 + \left(\frac{\delta P_{N_2}(z)}{P_{N_2}(z)}\right)^2\right]^{\frac{1}{2}},$$

where

$$\delta P_X = \left(P_{X,signal} + 2P_{X,noise}\right)^{\frac{1}{2}}. \quad (2)$$

The signal ($P_{X,\,signal}$) was obtained from the total backscatter signal by subtracting the background noise ($P_{X,\,noise}$), which was computed by taking the average of the total signal between the altitudes of 80 and 120 km, where atmospheric backscattering was expected to be negligible. The uncertainty of the calibration coefficient (δK) was estimated as the standard deviation of K, which was obtained from the comparison of uncalibrated MRL-derived data with the radiosonde data for the measurement period. As quality control (QC) of the derived data, we excluded data with uncertainty larger than 30% or w > 30 g/kg.

2.4 Calibration coefficient of the water vapor mixing ratio

To obtain the absolute value of w from the lidar signals, the calibration coefficient K of Eq. (1) is necessary. To obtain the value of K, several methods have been proposed and tested; they used external reference water vapor sensor measurements (e.g. radiosonde, GNSS, microwave radiometer, or sun-photometer) or external reference light source (e.g., diffuse sunlight or a standard lamp) and the effective Raman cross sections. A comprehensive review of these methods can be found elsewhere (Dai et al., 2018; David et al., 2017). In this study, we used the most conventional and reliable method by using radiosonde as described in Sect. 2.3. However, temporal change in K is a critical problem for long-term operation of the system, because if the temporal variation is large, K must be obtained frequently during the measurement period. We investigated this problem by examining the temporal variation in K values obtained by comparing uncalibrated MRL-derived w with collocated radiosonde measurements (see. Sec. 3.1 for the detail) obtained daily at 20:30 LST from August to December 2016 (Fig. 4). ~~Radiosondes (RS-11G, Meisei Electric. Co., Japan) were launched twice daily (8:30 and 20:30 LST) from an aerological~~

~~observatory located 80 m northeast of the MRL, and, according to the manufacturer, the measurement uncertainty of relative humidity by the RS-11G radiosonde is 5% in the lower troposphere and 7% in the upper troposphere (http://www.meisei.co.jp/english/products/RS-11G_E.pdf).~~ During the test period, the MRL system was operated nearly continuously at the Meteorological Research Institute in Tsukuba, except for short interruptions for flash lamp replacement (31 August and 24 October), power outages (18 August and 23 October), and trailer inspection (31 October to 6 November). We calculated K only for the nighttime (20:30 LST) data because at night the MRL measurement uncertainty was small between altitudes of 1 and 5 km (see Sect. 3.1). After 12 August, the value of K was nearly constant during the test period: mean ± standard deviation = 52.4 ± 2.1 (Fig. 4). Unfortunately, the reason for the abrupt change in K on 11 August from 57.4 ± 1.5 is unknown because we did not make any changes to the instrument at that time. Nevertheless, given the uncertainty of K (4% in this case), we may say that the MRL can be operated for at least 4 months without calibration. The possible reason for the variation of K is the variation of temperature in the trailer that can change the sensitivity of PMTs and center wavelength of IFs. During the experimental period, the variation of temperature in the trailer was at most ± 5 K, which corresponds to <6% variation of the effective Raman backscattering cross section ratio and thus K, assuming that the temperature variation of the sensitivity of PMT is <0.4%/K (Hamamatsu Photonics, 2017) and that of the filter CWL is < 0.0035 nm/K (FUJITOK, Japan, personal communication). To reduce the temperature variations, we need more stringent control of the temperature of the receiving system. We also examined the value of K before the system was moved from Tsukuba to the Tokyo Bay area (110 km or 70 km from Tsukuba) with that obtained after the move, from 15 June to 9 November 2017 (not shown). Before the system was moved, K was 46.9 ± 1.8, and afterward it was 43.1 ± 2.3, a change of 8.6% (we note also that after the telescope focus was readjusted in January 2017, the value of K changed from what it had been in 2016). These results indicate that the calibration coefficient should be determined before and after deployment of the system, and the average and standard deviation of those values should be used for K and δK.

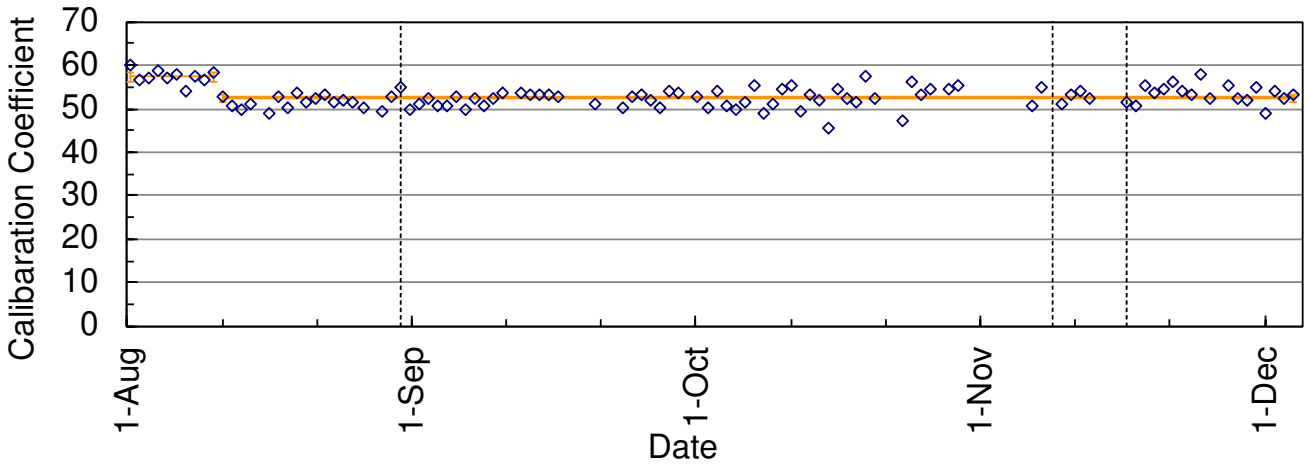

Figure 4. Temporal variation of the calibration coefficient of the water vapor mixing ratio (K) for the MRL obtained by comparison with collocated radiosonde measurements at 20:30 LST from August to December 2016. The horizontal orange lines show the averages before and after 12 August. The vertical dotted lines indicate dates on which the optical axis was adjusted.

2.5 Beam overlap correction for the Raman channels

Values of w calculated from the MRL signals for altitudes below 0.5 km were systematically lower than values obtained with the radiosonde when it was assumed that the beam overlap functions for the Raman water vapor and nitrogen channels were equal (i.e. $\frac{O_{H_2O}(z)}{O_{N_2}(z)} = 1$). When we compared the vertical distribution of the ratio of w obtained by radiosonde to that obtained

by the MRL without beam overlap correction (Fig. 5), we found considerable variation among individual profiles, but the average value of the ratio increased from 1 to 1.1 with a decrease of altitude from 0.7 to 0.1 km. Possible reasons for the difference in the overlap functions of the two Raman channels at low altitude are the difference in the optical paths (Fig. 1) and the spatial inhomogeneity of PMT sensitivity (Simeonov et al., 1999; Hamamatsu Photonics, 2017). To correct for the difference, we derived the ratio of beam overlap functions by comparing w obtained with the MRL under the assumption of $\frac{O_{H_2O}(z)}{O_{N_2}(z)} = 1$ with w obtained by radiosonde. Then, we calculated the mean vertical profile of the ratios and fitted a quadric curve to the profile for use in Eq. (1) to calculate w. The magnitude of the correction increased from 1% at 0.5 km altitude to 8% at 0.1 km. The uncertainty of the correction was estimated to be 8% from the standard deviation of the profiles. The possible reasons for the variation among the profiles are difference of the measurement period and temporal resolution (i.e. 20 minutes average for the lidar and approximately 1 second for the radiosonde), difference of the vertical resolution (i.e. 75 m for the lidar and 20–300 m that depends on the significant pressure level interval for the radiosonde, and lidar noise. The variation should be reduced if using the data measured above the lidar by using a kite (Totems and Chazette, 2016) or unmanned aerial vehicles.

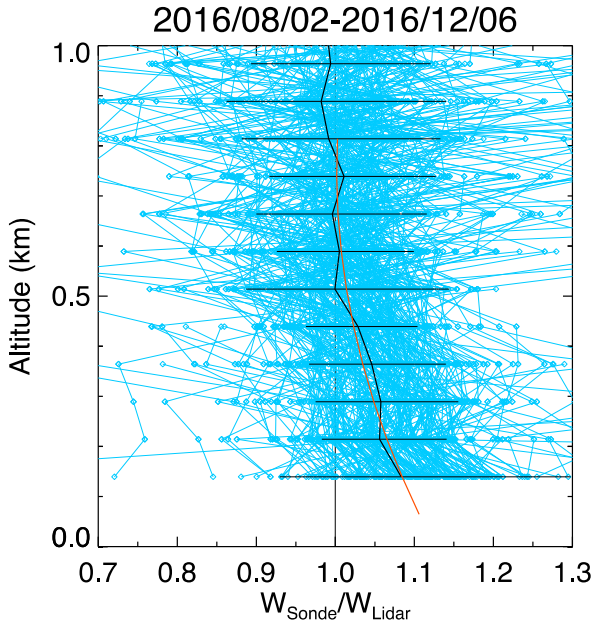

Figure 5. Vertical distribution of the ratio of w obtained by radiosonde (w_{Sonde}) to w obtained with the MRL system without beam overlap correction (w_{Lidar}) from 2 August to 6 December 2016. The individual profiles are shown by the thin blue lines with diamonds. The solid black line and the error bars are averages and standard deviations over 75 m height interval. A quadric curve (orange line) was fitted to the averaged values.

3 Validation results

To provide error estimates for the MRL system and characterize its performance, m~~M~~easurements for validation of the MRL system measurements were made on 120 days, from 2 August to 6 December 2016, over Tsukuba, Japan (36.06ºN, 140.12ºE). There have been many studies for the validation of the Raman lidar systems using robust approaches (e.g., Behrendt, et al., 2007, Bhawar et al., 2011, Herold et al., 2011). We validated MRL-derived w values ~~(described in Sect. 2.3)~~ by comparing them with collocated and coincident radiosonde, GNSS, and high-resolution local analysis (LA) data which are described below. ~~A GNSS receiver 80 m west of the MRL observed the carrier phase transmitted by GNSS satellites and estimated the precipitable water vapor (PWV) with a temporal resolution of 5 min during the validation period. The PWV value represents the vertically integrated water vapor content averaged over a horizontal distance of approximately 20 km around the antenna. See Shoji et al. (2004) for more details of the derivation method. The LA consists of hourly~~

~~meteorological data with a horizontal resolution of 2 km over Japan provided by the JMA. These data are obtained by a three-dimensional variational (3D-Var) data assimilation technique from hourly observation data from multiple sources, including surface measurements, satellites, and GNSS-derived PWV data. LA data provide initial conditions to local-scale NWP models used for 9-hour forecasts for aviation, weather warnings and advisories, and very short-range precipitation in and around Japan, provided every hour. The vertical resolution of the LA data is 45–868 m with 48 layers. See JMA (2016) for more details about the LA data.~~

3.1 Comparison with radiosonde measurements

Radiosondes (RS-11G, Meisei Electric. Co., Japan) were launched twice daily (8:30 and 20:30 LST) from an aerological observatory located 80 m northeast of the MRL, and, according to the manufacturer, the measurement uncertainty of relative humidity by the RS-11G radiosonde is 5% in the lower troposphere and 7% in the upper troposphere (http://www.meisei.co.jp/english/products/RS-11G_E.pdf).

3.1.1. Vertical distribution

We compared the vertical distribution of *w* obtained with the MRL with *w* obtained by radiosondes launched at 8:30 and 20:30 LST on 1 September 2016 over Tsukuba (Fig. 6). The ascent speed of the radiosondes was 5–6 m/s, so they reached a height of about 7 km after 20 min. The MRL data were accumulated over the 20 min following the radiosonde launch. The vertical resolution is reduced to 75 m below an altitude of 1 km and to 150 m above that to increase the signal-to-noise ratio (SNR) of the Raman backscatter signals. The values of *w* obtained with the MRL agreed well for the altitude range of 0.14–1.7 km with *w* obtained by radiosonde during 08:30–08:50 LST (Fig. 6a), and they agreed well for altitudes up to 6.2 km with radiosonde measurements made during 20:30–20:50 LST (Fig. 6b). Mean differences were 0.8 g/kg (7%) for the 08:30 LST radiosonde launch and 0.7 g/kg (15%) for the 20:30 LST launch. The maximum height of MRL measurements with an uncertainty of less than 30% was only 1.5 km in the daytime, because solar light reduces the SNR of the Raman backscatter signals; for example, at 08:30 LST on 1 September 2016, the solar zenith angle was 50° (Fig. 6a).

The altitude–time cross section of *w* obtained with the MRL on 1 September 2016 (Fig. 7) showed considerable diurnal moisture variation below an altitude of 3 km. The top height of a moist region (w > 12 g/kg) present below an altitude of 1 km during 00–03 LST increased to above 2 km as the sun rose during 03–06 LST. At midday, the top height of the moist region was probably above 1.5 km (although it cannot be seen because of the low SNR ratio in strong sunlight). After sunset, it remained at an altitude of 2.5 km, which probably corresponded to the top of a residual layer. The top of another moist region with *w* of 15 g/kg that emerged below an altitude of 1 km after 18 LST undulated with a vertical amplitude of a few hundred meters and a period of ~3 h. This result demonstrates the utility of the MRL system for monitoring the diurnal variation of water vapor in the lower troposphere, which is not captured by routine radiosonde measurements.

To test the long-term stability of the MRL system, we operated it for four months, from 2 August to 6 December 2016. After QC of the MRL data, the maximum measurement height was mostly ~1 km during the day throughout the measurement period, whereas at night when low, thick clouds were absent, it decreased from 6 km to 2.5 km over the measurement period (Fig. 8). We attribute this nighttime decrease to 1) a drop by almost half in the power of the laser transmitter during its continuous operation for three months, which caused the SNR of the signals to decrease, and 2) decreases in the water vapor concentration from summer to winter in the lower troposphere, which caused a decrease in the strength of Raman backscatter water vapor signals. As for the laser power, it increased from 110 mJ/pulse to 220 mJ/pulse after replacing the flash lamp and adjusting the angles of second and third harmonic crystals on 8 December 2017. As for the water vapor concentration, the monthly mean *w* values decreased from 17 to 4 g/kg at 1000 hPa and from 8 to 1 g/kg at 700 hPa between August and December in 2016.

In general, vertical distributions of w obtained with the MRL system agreed well with radiosonde measurements (Fig. 9). However, the MRL- and radiosonde-derived values sometimes differed considerably from LA data for the same dates (e.g. between 2.5 and 3.5 km at 20:30 LST on 9 August, between 1.5 and 2.5 km at 20:30 LST on 16 September, and between 0.5 and 1.2 km at 20:30 LST on 2 December 2016). More detailed analysis will be given in Sect. 3.3.

To study the height dependence of the difference ($w_{Lidar} - w_{Sonde}$), we examined the vertical variation of the mean difference at intervals of 500 m (Fig. 10). The mean difference was less than 1 g/kg (10%) below an altitude of 6 km at night and below 1 km in the daytime. Above these altitudes, the MRL values were higher than the radiosonde-derived values. Possible reasons for the larger differences at higher altitudes are 1) the small number of data points in those regions (Fig. 10d), which caused the statistical significance to be low, 2) the difference in the air parcel measured by the two instruments, because as they ascended the radiosondes were sometimes blown several kilometers or more from the MRL position by horizontal winds, particularly above an altitude of 6 km at night, and 3) the generation of spurious Raman signals above 1 km by high solar background radiation in the daytime, as will be discussed in Sect. 3.1.2. The influence of the temperature dependence of the Raman cross section (e.g. Whiteman, 2003) is negligible for the MRL because the variation is estimated to be 0.5% for the temperature range of 253–303 K.

(a) (b)

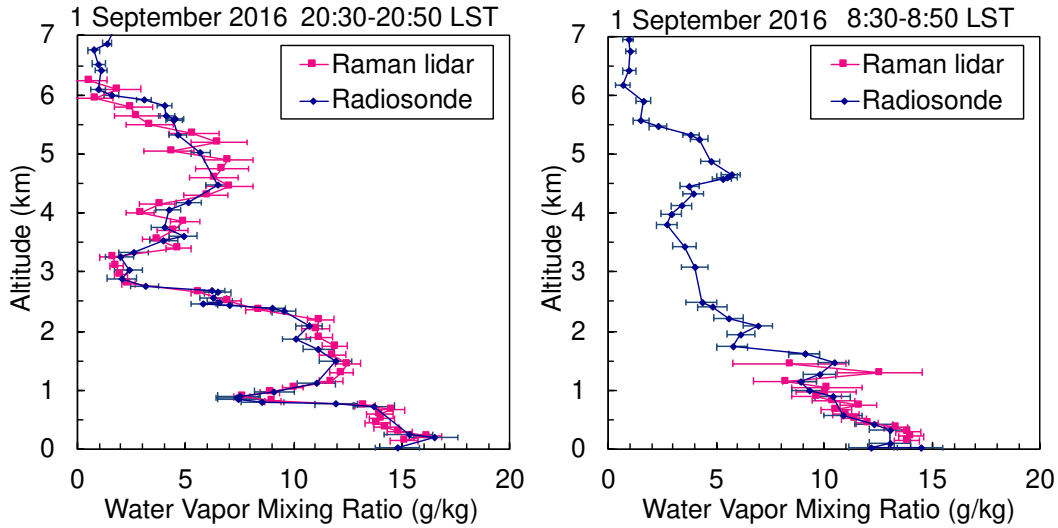

Figure 6. Vertical distributions of the water vapor mixing ratio obtained with the MRL (magenta), radiosonde (dark blue) on 1 September 2016 over Tsukuba. The measurement periods for the MRL were (a) 08:30–08:50 and (b) 20:30–20:50 LST, and the radiosondes were launched at (a) 8:30 LST and (b) 20:30 LST. MRL data with uncertainty of less than 30% are plotted.

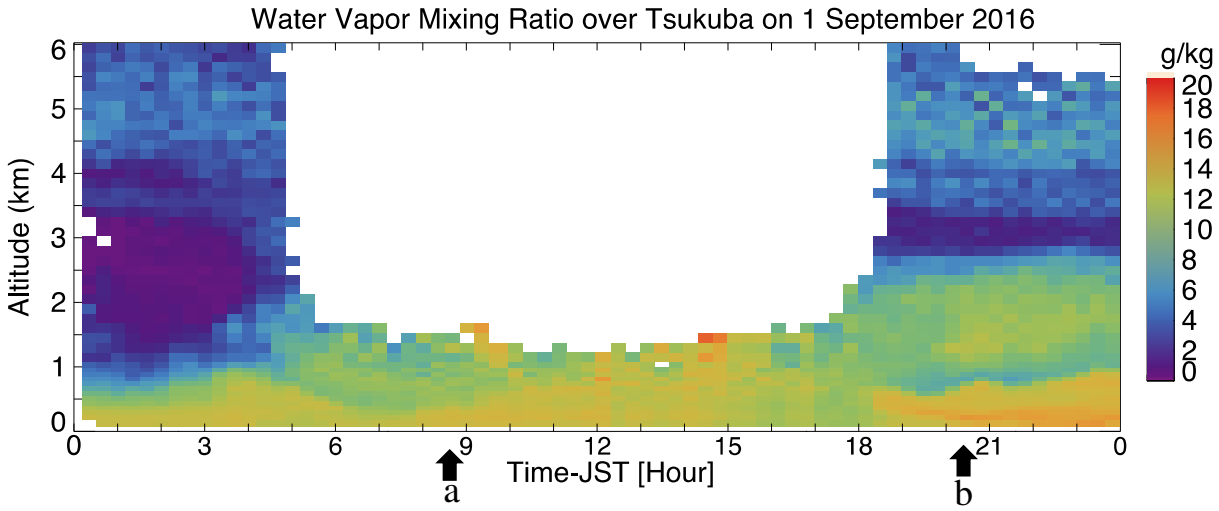

Figure 7. Altitude–time cross section of water vapor mixing ratios obtained with the MRL on 1 September 2016. Data with uncertainty of less than 30% are plotted. Arrows at the bottom show the start of the measurement periods for the data shown in Fig. 6.

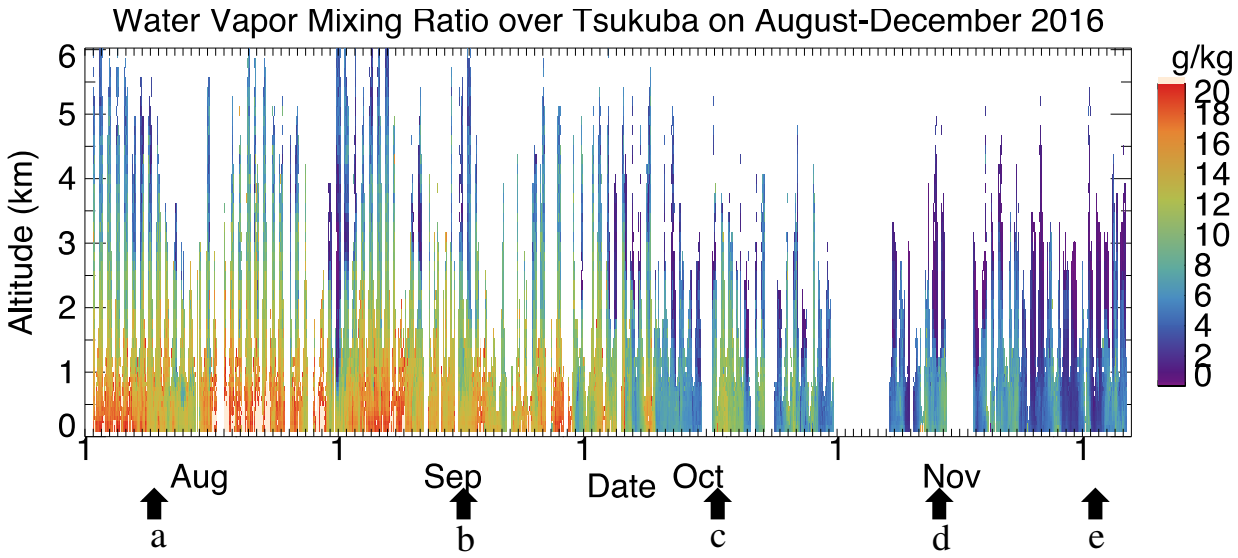

Figure 8. Altitude–time cross section of water vapor mixing ratios obtained with the MRL from 2 August to 6 December 2016. Data with uncertainty of less than 30% are plotted. Arrows at the bottom show the dates for which vertical profiles are shown in Fig. 9.

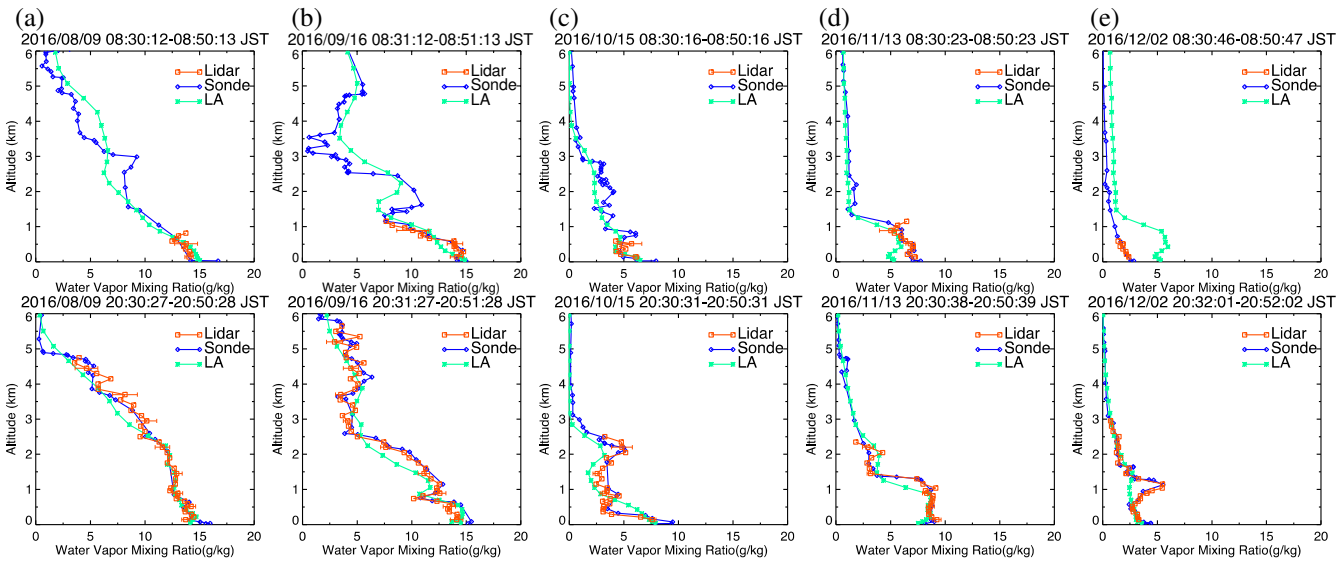

Figure 9. Vertical distributions of water vapor mixing ratios obtained with the MRL (orange) and radiosondes (blue) compared with local analysis data (green) for 08:30 LST (upper panel) and 20:30 LST (bottom panels) on (a) 9 August, (b) 16 September, (c) 15 October, (d) 13 November, and (e) 2 December 2016.

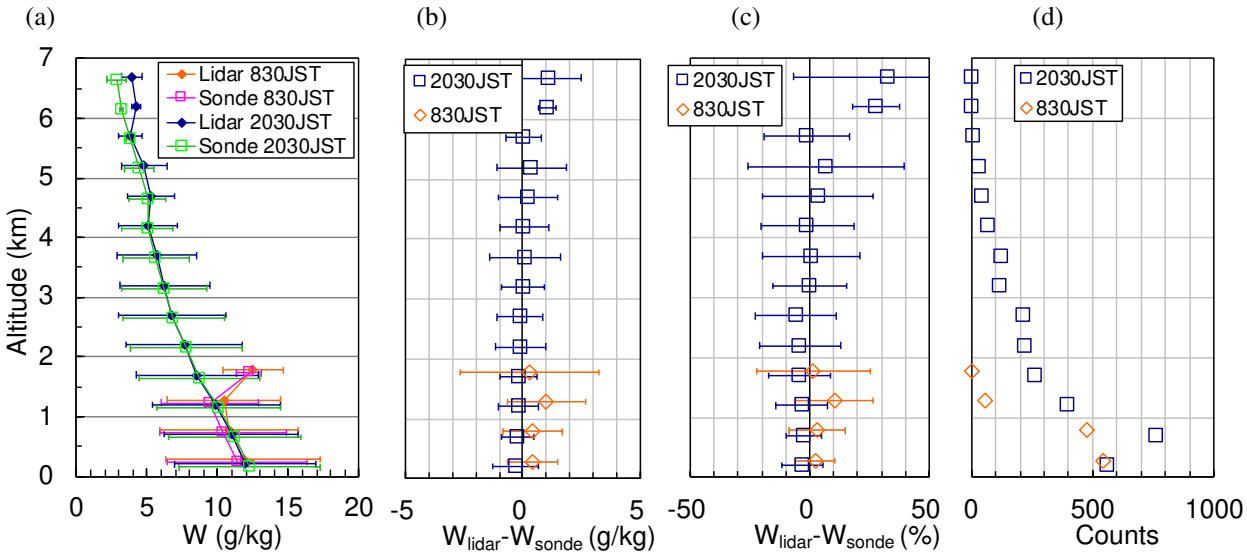

Figure 10. Vertical variations of (a) mean w_{Lidar} values (diamonds) and w_{Sonde} (open squares) values at intervals of 500 m for 20:30 LST and 08:30 LST from 2 August to 6 December 2016, and their (b) absolute and (c) relative differences. Symbols and error bars in (a)–(c) show means and standard deviations. (d) The number of data points at each altitude.

3.1.2 Scatter plot comparison

After the data were screened for QC, we compared w values obtained with the MRL and by radiosonde from 2 August to 6 December 2016 in 110 vertical profiles for 20:30 LST and 113 for 08:30 LST (Fig. 11). For this comparison, the radiosonde data were linearly interpolated to the heights of the MRL data. Note that the maximum altitude of the comparison for 08:30 LST (1.9 km) was lower than that for 20:30 LST (6.85 km) because, owing to their large uncertainty, daytime data at higher altitudes were excluded by the QC screening. The MRL-derived w (w_{Lidar}) values agreed with the radiosonde-derived values (w_{Sonde}) over the range from 0 to 20 g/kg (Fig. 11). A geometric mean regression analysis conducted by assuming that w_{Sonde} = slope $\times w_{Lidar}$ + bias yielded a slope of 0.~~990~~989 with the statistical uncertainty of ±0.002 and an intercept of –0.002 ± 0.018 for the 20:30 LST (Fig. 11a) and a slope of 1.~~045~~051 ± 0.004 and an intercept of –0.005 ± 0.053 g/kg for 08:30 LST (Fig. 11b). To examine the dependence of the difference in w ($w_{Lidar} - w_{Sonde}$) on the magnitude of w_{Sonde}, we plotted ($w_{Lidar} - w_{Sonde}$) as a function of w_{Sonde}, as well as the means and standard deviations of ($w_{Lidar} - w_{sonde}$), at intervals of 2.5 g/kg (Figs. 11c and 11d). As a result, we found no significant bias in the difference for w_{Sonde} ranging from less than 20 g/kg at night to less than 15 g/kg in the daytime (i.e., mean differences were smaller than 0.3 g/kg). In contrast, we found positive biases for larger w_{Sonde} value ranges; the bias was 1.7 g/kg at 08:30 LST for w ranging from 17.5 to 20 g/kg. A possible reason for the daytime bias at high values of w_{Sonde} is that high solar background radiation generated spurious noise spikes and high photon counts in Raman water vapor signals above an altitude of 1 km that were not rejected by QC. We are investigating the method to reject such data by QC, although they have small impacts on the water vapor fields analyzed from the data assimilation because their measurement errors are large.

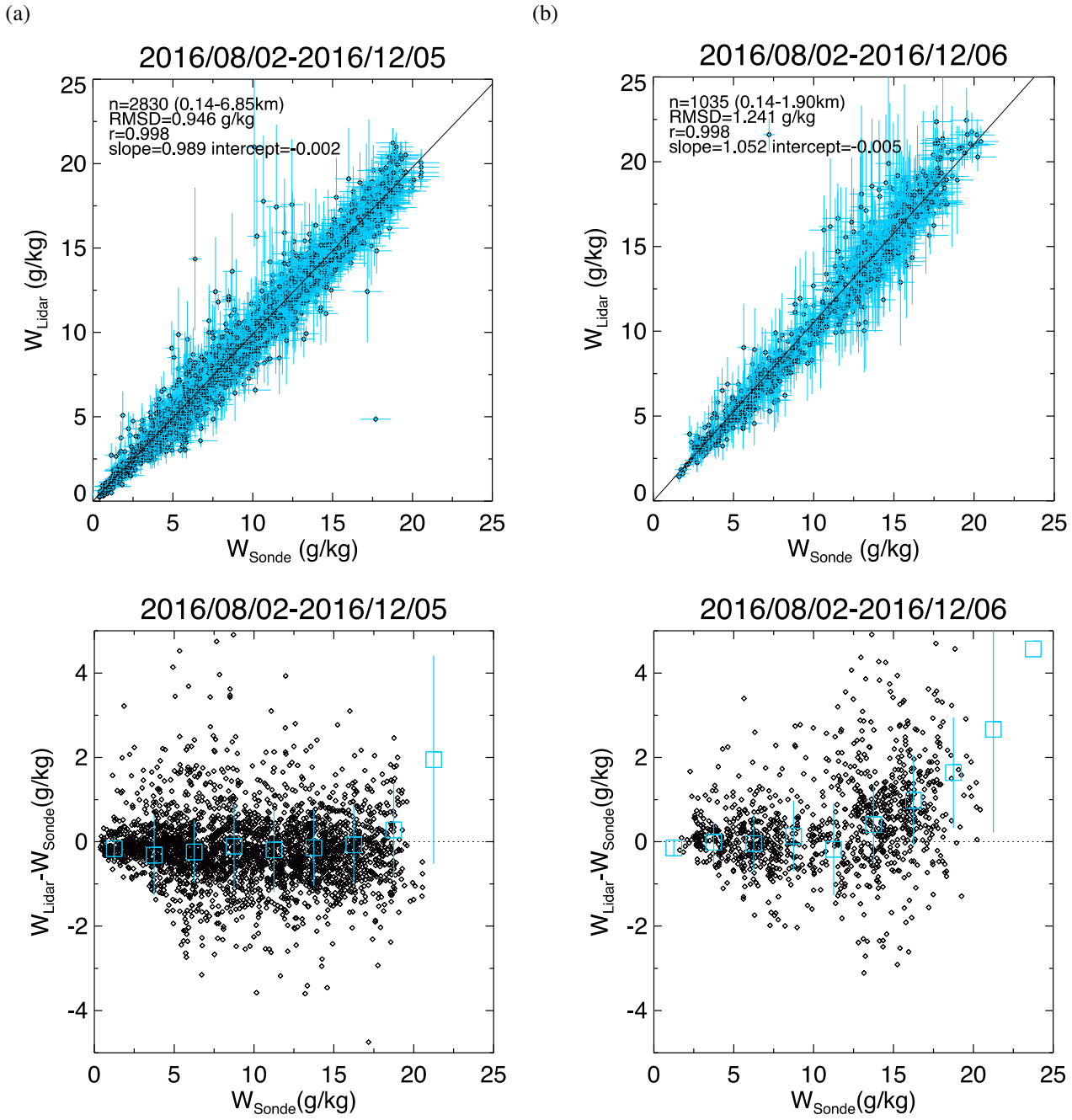

Figure 11. (Top panels) Scatter plots of w obtained with the MRL (w_{Lidar}) versus w obtained with radiosondes (w_{Sonde}) at (a) 20:30 LST and (b) 08:30 LST from 2 August to 6 December 2016. (Bottom panels) Scatter plots of the difference ($w_{Lidar} - w_{Sonde}$) as a function of w_{Sonde} at (c) 20:30 LST and (d) 08:30 LST. Blue symbols show the means, and the blue lines show the standard deviations of the difference at intervals of 2.5 g/kg. Data points with an MRL measurement uncertainty of less than 30% are plotted.

3.2 Comparison with GNSS PWV data

To validate the MRL measurement data for times when coincident radiosonde data were unavailable, we compared the MRL-derived PWV with PWV values obtained from GNSS data. The GNSS receiver was located 80 m west of the MRL. It observed the carrier phase transmitted by GNSS satellites from which the precipitable water vapor (PWV) was estimated with a temporal resolution of 5 min during the validation period. The PWV value represents the vertically integrated water vapor content averaged over a horizontal distance of approximately 20 km around the antenna. See Shoji et al. (2004) for more details of the derivation method.To obtain PWV from the MRL data, we computed the vertical profile of the water vapor density from MRL-

derived *w* and atmospheric density obtained by the radiosonde closest in time to the MRL measurement period, and vertically integrated the water vapor density from an altitude of 0.1 km to the maximum height with a measurement uncertainty of less than 30%. Below 0.1 km, we interpolated the *w* data to the ground level in-situ measurement. Then we compared the temporal variations of PWV obtained with the MRL with those obtained from GNSS data from August to December 2016 (Fig. 12). So that this comparison would be meaningful, we excluded MRL data obtained when the maximum measurement height was lower than 5 km; as a result, mostly nighttime lidar values obtained when low, thick clouds were absent were used in the comparison. The temporal resolution of the GNSS data was reduced by averaging from 5 min (original GNSS resolution) to 20 min to match the resolution of the MRL data.

The temporal variation of MRL-derived PWV was similar to that of the GNSS-derived PWV (Fig. 12). In summer (August–September), when a moist air mass from the Pacific Ocean covered the observation area, the PWV values were mostly higher than 30 mm. In autumn and winter (October–December), when a dry air mass from the Asian continent prevailed, the PWV values were mostly lower than 20 mm. We note that the number of available lidar PWV data was smaller in autumn and winter than in summer because the decrease in the laser power as mentioned before (Sect. 3.1.1) and because in autumn and winter the Raman backscatter signal tends to be weak by the low water vapor concentration in the middle troposphere. The regression analysis of PWV derived from MRL data against GNSS-derived PWV showed a strong positive correlation (correlation coefficient 0.991; Fig. 13a) between them, but many of the MRL-derived PWV values were lower, most by up to 5 mm, than the GNSS-derived values (Fig. 13b). The most plausible reason for the lower MRL-derived PWV values is that the MRL did not always measure the entire water vapor column. In addition, both positive and negative differences could be caused by the measured air masses being different (see Sect. 3). The difference in PWV would be large if large horizontal inhomogeneity of the water vapor concentration existed in the observation area. Shoji et al. (2015) utilized the slant path delay of the GNSS signal to estimate the horizontal inhomogeneity of water vapor on a scale of several kilometers around the measurement site. The use of a technique that combines MRL and GNSS observations for monitoring the vertical and horizontal distributions of water vapor holds promise, and the development of such a technique is our future task.

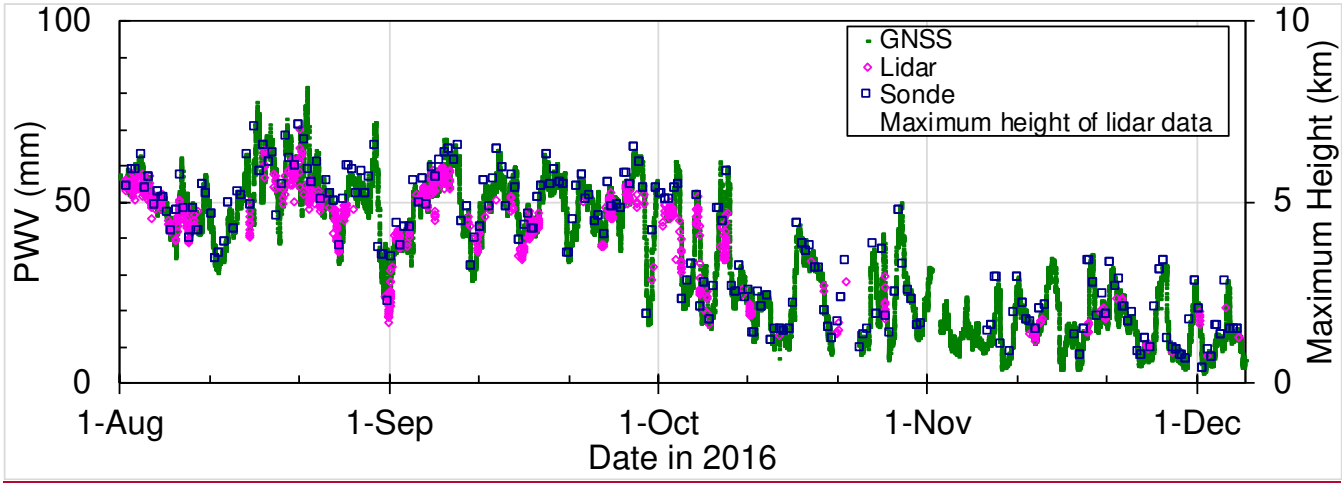

Figure 12. Temporal variations of PWV obtained with lidar (magenta diamonds), GNSS (green dots), and radiosonde (blue squares) from 2 August to 6 December 2016 over Tsukuba. Data with measurement uncertainties of less than 10% that were obtained when the maximum MRL measurement height exceeded 5 km (light blue asterisks) are plotted.

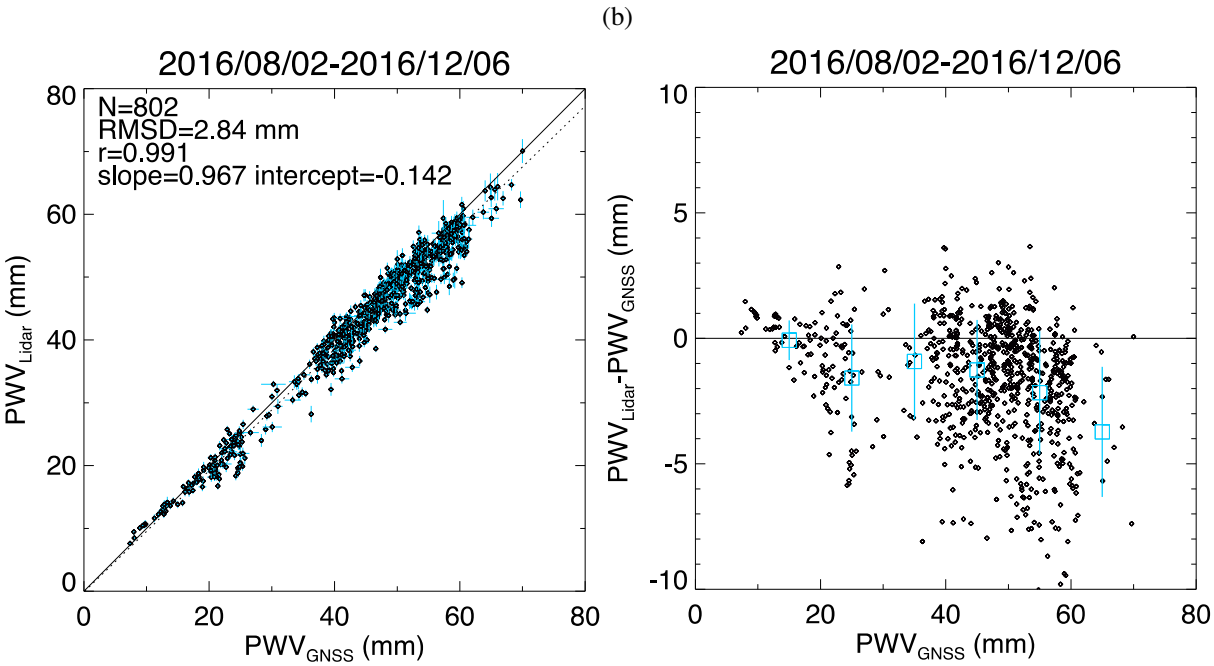

Figure 13. Scatter plots (a) of PWV obtained with the MRL system against PWV obtained from GNSS data from 2 August to 6 December 2016 and (b) their difference ($PWV_{Lidar} - PWV_{GNSS}$) versus PWV_{GNSS}. In (b), the open squares and vertical lines show the means and standard deviations of the difference at intervals of 10 mm.

3.3 Comparison with local analysis data

We compared hourly MRL values of *w* with LA data because the primary purpose of our MRL measurement was to improve the initial condition of the water vapor field of the NWP model. The LA consists of hourly meteorological data with a horizontal resolution of 2 km over Japan provided by the JMA. These data are obtained by a three-dimensional variational (3D-Var) data assimilation technique from hourly observation data from multiple sources, including surface measurements, satellites, and GNSS-derived PWV data. LA data provide initial conditions to local-scale NWP models used for 9-hour forecasts for aviation, weather warnings and advisories, and very short-range precipitation in and around Japan, provided every hour. The vertical resolution of the LA data is 45–868 m with 48 layers. See JMA (2016) for more details about the LA data.

3.3.1 Vertical distributions

~~We compared hourly MRL values of *w* with LA data because the primary purpose of our MRL measurement was to improve the initial condition of the water vapor field of the NWP model.~~ Our comparison of vertical variations in *w* obtained with the MRL system with *w* derived from the LA (Fig. 9) showed the higher values of the MRL than the LA data. The statistics of the comparison showed that the MRL values were higher by up to 1.1 g/kg (25%) over the entire altitude range (Fig. 15). In addition, the magnitude of the difference ($w_{Lidar} - w_{LA}$) was larger than the difference with radiosonde values ($w_{Lidar} - w_{Sonde}$) (Fig. 10). This result suggests that the assimilation of MRL data has the potential to improve the initial conditions provided to the NWP model.

3.3.2 Scatter plot comparison

Figure 14 shows the scatter plot of w obtained with MRL. For this comparison, the MRL data were linearly interpolated to the heights of the LA data. The result revealed that the root mean square difference (RMSD) (1.~~367~~ 390 g/kg) was larger than that obtained when we compared MRL values with nighttime radiosonde values (0.~~968~~ 989 g/kg; Fig. 11a). Moreover, the MRL-derived *w* values were consistently higher, by 0.2–0.8 g/kg (1–11%), than those derived by LA for *w* in the range of 0–22.5

g/kg (Fig. 14b). We also compared LA data with the radiosonde data for the same period (not shown) and found that the mean LA data at intervals of 2.5 g/kg differed from the radiosonde data by –0.2 to 0.9 g/kg (3–11%). We infer that the LA data used in this comparison had a negative bias because the accuracy of the radiosonde relative humidity measurements was 5–7%. The differences with the LA data can be related to local effects and thus to the representativeness of the measurement site at the mesoscale. They can also be due to a problem in the assimilation process if it does not integrate well the error matrices.

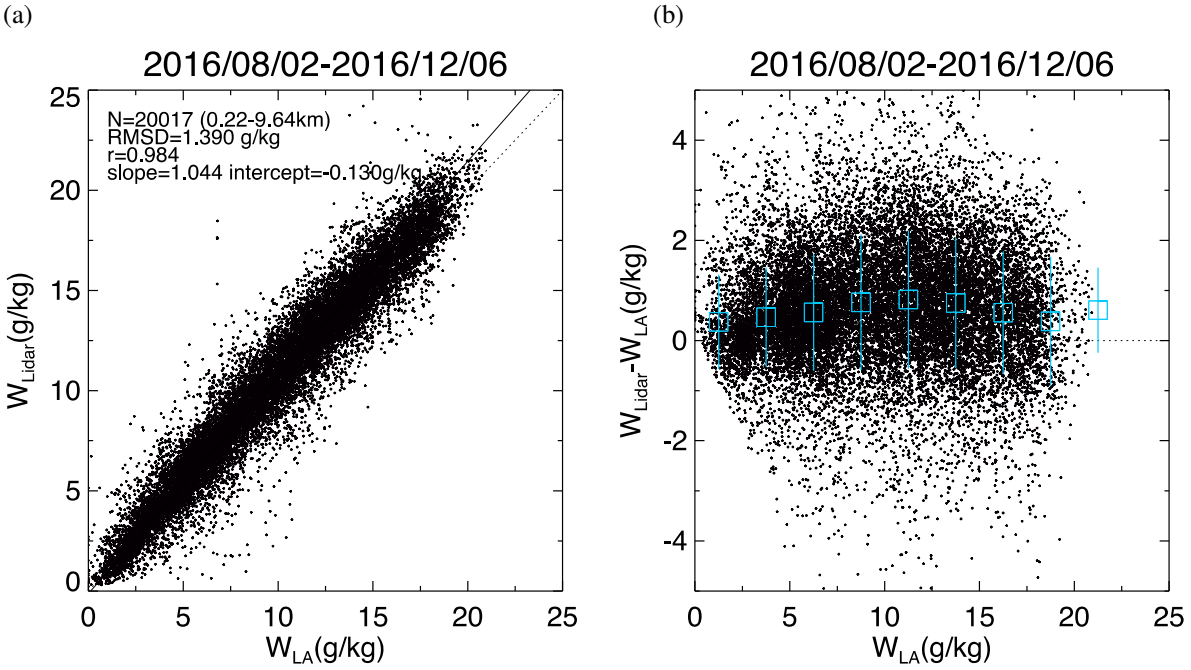

Figure 14. Scatter plots of (a) w obtained with the MRL (w_{Lidar}) versus w obtained from the local analysis (w_{LA}) and (b) their difference ($w_{\mathrm{Lidar}} - w_{\mathrm{LA}}$) as a function of w_{LA} from 2 August to 6 December 2016. In (b), the blue open squares and vertical lines show means and standard deviations of the difference at intervals of 2.5 g/kg.

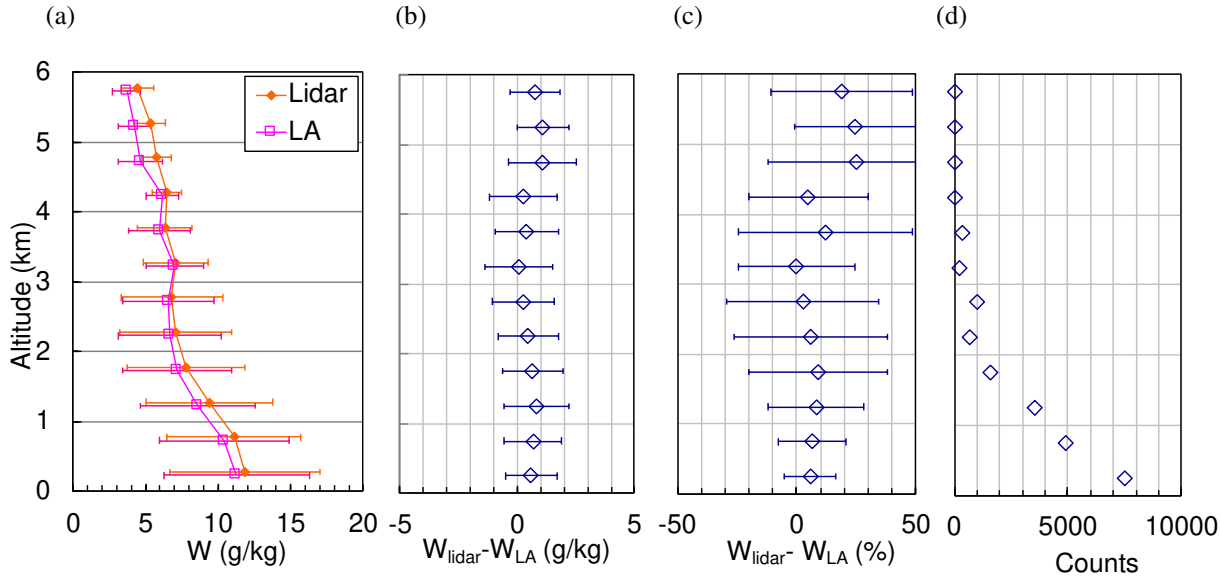

Figure 15. Vertical variations of (a) mean values and standard deviations of w obtained with the MRL (w_{Lidar}) and from the local analysis (w_{LA}) at 500-m intervals and their (b) absolute and (c) relative differences from 2 August to 6 December 2016. Symbols and error bars in (b) and (c) show the means and standard deviations of the difference. (d) The number of data points at each altitude.

3.4 Summary of the validation results and outlook

Table ~~3~~2 summarizes the results of our comparisons of water vapor measurements obtained by the MRL and other instruments or local analyses. The correlation was highest and the RMSD was smallest when MRL-derived *w* was compared with *w* obtained by radiosonde at night. This result was probably because 1) the MRL system was calibrated by using radiosonde data, 2) the instruments measured the same quantity (*w*), and 3) the measurement performance of the MRL was best at night. The agreement with radiosonde data was not as good in the daytime as it was at night because of the measurement uncertainty of *w* was larger in the daytime, even though the slope and intercept of the regression analysis did not differ significantly between daytime and nighttime measurements. The MRL-derived PWVs at night were slightly lower than those derived from GNSS data because of the measurement range limitation of the MRL system. The regression analysis of MRL-derived *w* versus LA data showed that the magnitudes of the deviation of the slope from 1 and the deviation of the intercept from zero were larger than those obtained in the analysis with radiosonde data, and the correlation coefficient was the lowest among the comparisons. From these results, we can ~~conclude~~ expect that assimilation of MRL-derived *w* after QC can improve the initial conditions of the NWP model for heavy rain forecasting. In fact, ~~A~~a first data assimilation experiment of the MRL-derived vertical profiles of *w* into the JMA-NHM using the three-dimensional LETKF for the heavy rainfall forecasting has been reported by Yoshida et al. (2018a), who showed a positive impact on the analyzed and forecast humidity fields on the Kanto Plain on 17 August 2016. More detailed description of the assimilation experiments will follow soon (Yoshida et al. 2018b).

Despite the potential usefulness of the MRL-measured data for the weather forecasting, the MRL cannot measure the water vapor inside and above optically thick clouds. To overcome this disadvantage, it is important to use synergistic approaches with different instruments such as GNSS, microwave radiometer, radiosonde to measure the water vapor distribution even under cloudy conditions (e.g., Foth and Pospichal, 2017).

Table ~~3~~2. Results of water vapor measurements by the MRL compared with data obtained by other instruments or from local analyses. Values in the parentheses of slope and intercept are the statistical uncertainties.

Data type	Time (LST)	Slope	Intercept (g/kg)	Correlation coefficient	RMSD (g/kg)	No. of data points
Radiosonde	20:30	0.~~990~~989 (0.002)	–0.002 (0.018)	0.998	0.~~968~~946	~~2836~~2830
	08:30	1.~~045~~051 (0.004)	–0.005 (0.053)	0.997~~8~~	1.~~507~~284	~~1107~~1081
	All	1.00~~3~~9 (0.002)	–0.001 (0.017)	0.~~997~~998	~~0.983~~1.050	~~4903~~3911
GNSS (PWV)	0:00–23:00	0.967 (0.012)	–0.142 mm (0.142 mm)	0.991	2.84 mm	802
LA	00:00–23:00 (hourly)	1.~~033~~044 (0.003)	~~–0.086~~0.202 (0.014)	0.98~~3~~4	1.~~367~~390	~~20060~~20017

4 Conclusion

We developed a low-cost, automated -compact mobile Raman lidar system for measuring the vertical distribution of the water vapor mixing ratio *w* in the lower troposphere, which is easy to ~~to improve the accuracy and lead time of heavy rainfall prediction. The MRL can~~ be ~~easily~~ deployed to remote sites and is capable of unattended operation for several months. Our comparison of the MRL-derived *w* values with those obtained with collocated radiosondes showed that they agreed within

10% and RMSD with 0.98 g/kg between altitudes of 0.14 and 5–6 km at night and between altitudes of 0.14 and 1.5 km in the daytime. The calibration coefficient of the MRL showed no significant temporal variation during 4 months of continuous operation in 2016. A small correction for beam overlap was necessary below 0.5 km. The MRL-derived precipitable water vapor values obtained at night when low clouds were absent and the maximum heights of the MRL measurement exceeded 5 km were slightly lower than those obtained from GNSS data. The fact that the MRL-derived *w* values were at most 1 g/kg (25%) larger than those in the local analysis data suggests that assimilation of the MRL data can improve the initial condition of the water vapor distribution in the lower troposphere of the NWP model. Although the MRL system was originally developed for heavy rain forecasting, it can also be utilized for the study of water vapor in the lower troposphere such as boundary layer structure and cloud formation.

~~The impact of using the lidar data with the nonhydrostatic mesoscale model for simulating heavy rainfall in the Kanto area in summer 2016 reported by Yoshida et al. (2018a) showed a positive impact on the humidity fields that were analyzed and forecasted by the model.~~

The measurement altitude of the current Raman lidar system is limited to 1.5 km in the daytime. Although this limitation might not preclude the use of data from the system for heavy rain forecasting and the other applications, it would be better to expand the measurement height ~~range because the mixed layer, where the inflow of the large amount of water vapor that causes heavy rain mostly occurs, can be as high as 2 km. Moreover, humidity in the middle troposphere affects the development of cumulus convections to the upper troposphere~~. To detect water vapor in the middle troposphere in the daytime, a diode laser-based differential absorption lidar might be useful because it can continuously measure the water vapor concentration up to an altitude of 3 km both in the daytime and at night (Repasky et al., 2013; Spuler et al., 2015; Pham Le Hoai et al., 2016). ~~We are also developing such a system (Pham Le Hoai et al., 2016) to improve the model forecast skill for heavy rainfall in urban areas.~~

Acknowledgements

We used radiosonde data measured by the Japan Meteorological Agency (downloaded from http://www.data.jma.go.jp/obd/stats/etrn/upper/index.php).

References

Behrendt, A., V. Wulfmeyer, H. Bauer, T. Schaberl, P. Di Girolamo, D. Summa, C. Kiemle, G. Ehret, D.N. Whiteman, B.B. Demoz, E.V. Browell, S. Ismail, R. Ferrare, S. Kooi, and J. Wang: Intercomparison of Water Vapor Data Measured with Lidar during IHOP 2002. Part I: Airborne to Ground-Based Lidar Systems and Comparisons with Chilled-Mirror Hygrometer Radiosondes, J. Atmos. Oceanic Technol., 24, 3–21, https://doi.org/10.1175/JTECH1924.1, 2007.

Bhawar R, Di Girolamo P, Summa D, Flamant C, Althausen D, Behrendt A, Kiemle C, Bosser P, Cacciani M, Champollion C, Di Iorio T, Engelmann R, Herold C, Müller D, Pal S, Wirth M, Wulfmeyer V.: The water vapour intercomparison effort in the framework of the Convective and Orographically- induced Precipitation Study: airborne-to-ground-based and airborne-to-airborne lidar systems, Q. J. R. Meteorol. Soc., 137: 325–348. doi:10.1002/qj.697, 2011.

Bielli, S., Grzeschik, M. , Richard, E. , Flamant, C. , Champollion, C. , Kiemle, C. , Dorninger, M. and Brousseau, P.: Assimilation of water-vapour airborne lidar observations: impact study on the COPS precipitation forecasts, Q. J. R. Meteorol. Soc., 138: 1652-1667., doi:10.1002/qj.1864, 2012.

Bucholtz, A., : Rayleigh-scattering calculations for the terrestrial atmosphere, Appl. Opt., 34, 2765-2773, 1995

Chazette, P., Marnas, F., and Totems, J.: The mobile water vapor aerosol Raman LIdar and its implication in the framework of the HyMeX and ChArMEx programs: application to a dust transport process, Atmos. Meas. Tech., 7, 1629-1647, https://doi.org/10.5194/amt-7-1629-2014, 2014.

Dai, G., Althausen, D., Hofer, J., Engelmann, R., Seifert, P., Bühl, J., Mamouri, R.-E., Wu, S., and Ansmann, A.: Calibration of Raman lidar water vapor profiles by means of AERONET photometer observations and GDAS meteorological data, Atmos. Meas. Tech., 11, 2735-2748, https://doi.org/10.5194/amt-11-2735-2018, 2018.

David, L., Bock, O., Thom, C., Bosser, P., and Pelon, J.: Study and mitigation of calibration factor instabilities in a water vapor Raman lidar, Atmos. Meas. Tech., 10, 2745-2758, https://doi.org/10.5194/amt-10-2745-2017, 2017.

Dinoev, T., Simeonov, V., Arshinov, Y., Bobrovnikov, S., Ristori, P., Calpini, B., Parlange, M., and van den Bergh, H.: Raman Lidar for Meteorological Observations, RALMO – Part 1: Instrument description, Atmos. Meas. Tech., 6, 1329-1346, https://doi.org/10.5194/amt-6-1329-2013, 2013.

Engelmann, R., Kanitz, T., Baars, H., Heese, B., Althausen, D., Skupin, A., Wandinger, U., Komppula, M., Stachlewska, I. S., Amiridis, V., Marinou, E., Mattis, I., Linné, H., and Ansmann, A.: The automated multiwavelength Raman polarization and water-vapor lidar PollyXT: the neXT generation, Atmos. Meas. Tech., 9, 1767-1784, https://doi.org/10.5194/amt-9-1767-2016, 2016.

Goldsmith, J. E. M., F. H. Blair, S. E. Bisson, and D. D. Turner: Turn-key Raman lidar for profiling atmospheric water vapor, clouds, and aerosols, Appl. Opt., 37, 4979-4990, 1998.

Grzeschik, M., H. Bauer, V. Wulfmeyer, D. Engelbart, U. Wandinger, I. Mattis, D. Althausen, R. Engelmann, M. Tesche, and A. Riede: Four-imensional Variational Data Analysis of Water Vapor Raman Lidar Data and Their Impact on Mesoscale Forecasts, J. Atmos. Oceanic Technol., 25, 1437–1453, https://doi.org/10.1175/2007JTECHA974.1, 2008.

Herold, C., D. Althausen, D. Müller, M. Tesche, P. Seifert, R. Engelmann, C. Flamant, R. Bhawar, and P. Di Girolamo: Comparison of Raman Lidar Observations of Water Vapor with COSMO-DE Forecasts during COPS 2007. Wea. Forecasting, 26, 1056–1066, https://doi.org/10.1175/2011WAF2222448.1 , 2011.

Japan Meteorological Agency (JMA), Climate change monitoring Report 2016, 93pp., downloaded from http://www.jma.go.jp/jma/en/NMHS/indexe_ccmr.html, 2017.

Hamamatsu Photonics, Photomultiplier Tube Handbook, 3rd Ed., p59-62, downloaded from http://www.hamamatsu.com/resources/pdf/etd/PMT_handbook_v3aE.pdf, 2017.

Kato, T., Representative Height of the Low-Level Water Vapor Field for Examining the Initiation of Moist Convection Leading to Heavy Rainfall in East Asia. J. Meteor. Soc. Japan, 82, 69–83, https://doi.org/10.2151/jmsj.2018-008, 2018.

Kunii, M.: Mesoscale data assimilation for a local severe rainfall Event with the NHM–LETKF System. Wea. Forecasting, 29, 1093–1105, https://doi.org/10.1175/WAF-D-13-00032.1, 2014.

Leblanc, T., McDermid, I. S., and Walsh, T. D.: Ground-based water vapor Raman lidar measurements up to the upper troposphere and lower stratosphere for long-term monitoring, Atmos. Meas. Tech., 5, 17-36, https://doi.org/10.5194/amt-5-17-2012, 2012.

Melfi, S. H., J. D. Lawrence, M. P. McCormick: Observation of Raman scattering by water vapor in the atmosphere, Appl. Phys. Lett., 15, 295–297, 1969.

Phong Pham Le Hoai, M. Abo, T. Sakai: Development of field-deployable Diode-laser-based water vapor DIAL, EPJ Web of Conferences 119 05011, doi: 10.1051/epjconf/20161190501, 2016.

Reichardt, J., U. Wandinger, V. Klein, I. Mattis, B. Hilber, and R. Begbie: RAMSES: German Meteorological Service autonomous Raman lidar for water vapor, temperature, aerosol, and cloud measurements, Appl. Opt., 51, 8111-8131, 2012.

Repasky, K.S., Moen, D., Spuler, S., Nehrir, A.R., Carlsten, J.L.: Progress towards an autonomous field deployable diode-laser-based differential absorption lidar (DIAL) for profiling water vapor in the lower troposphere. Remote Sens., 5, 6241-6259, 2013.

Saito, K., J. Ishida, K. Aranami, T. Hara, T. Segawa, M. Narita and Y. Honda: Nonhydrostatic atmospheric models and operational development at JMA. J. Meteor. Soc. Japan, 85B, 271-304, 2007.

Sakai, T., T. Nagai, M. Nakazato, T. Matsumura, N. Orikasa, and Y. Shoji: Comparisons of Raman lidar measurements of tropospheric water vapor profiles with radiosondes, hygrometers on the meteorological observation tower, and GPS at Tsukuba, Japan. J. Atmos. Oceanic Technol., 24, 1407–1423, https://doi.org/10.1175/JTECH2056.1, 2007.

Shoji, Y., and Coauthors: Tsukuba GPS dense net campaign observation: Improvement of GPS analysis of slant path delay by stacking one-way post fit phase residuals. J. Meteor. Soc. Japan, 82, 301–314, 2004.

Shoji, Y., W. Mashiko, H. Yamauchi, and E. Sato: Estimation of local-scale precipitable water vapor distribution around each GNSS station using slant path delay: Evaluation of a tornado case using high-resolution NHM. SOLA, 11, 31–35, doi:https://doi.org/10.2151/sola.2015-008, 2015.

Simeonov, V., G. Larcheveque, P. Quaglia, H. van den Bergh, and B. Calpini: Influence of the photomultiplier tube spatial uniformity on lidar signals, Appl. Opt., 38, 5186-5190, 1999.

Spuler, S. M., Repasky, K. S., Morley, B., Moen, D., Hayman, M., and Nehrir, A. R.: Field-deployable diode-laser-based differential absorption lidar (DIAL) for profiling water vapor, Atmos. Meas. Tech., 8, 1073-1087, https://doi.org/10.5194/amt-8-1073-2015, 2015.

Totems, J. and Chazette, P.: Calibration of a water vapour Raman lidar with a kite-based humidity sensor, Atmos. Meas. Tech., 9, 1083-1094, https://doi.org/10.5194/amt-9-1083-2016, 2016.

Turner, D.D., J.E. Goldsmith, and R. A. Ferrare: Development and Applications of the ARM Raman Lidar, Meteorological Monographs, 57, 18.1–18.15, https://doi.org/10.1175/AMSMONOGRAPHS-D-15-0026.1, 2016.

Whiteman, D. N., S. H. Melfi, and R. A. Ferrare: Raman lidar system for the measurement of water vapor and aerosols in the Earth's atmosphere. Appl. Opt. 31, 3068-3082, 1992.

Whiteman, D. N.: Examination of the traditional Raman lidar technique. I. Evaluating the temperature-dependent lidar equations. Appl. Opt. 42, 2571–2592, 2003.

Whiteman, D. N., Cadirola, M., Venable, D., Calhoun, M., Miloshevich, L., Vermeesch, K., Twigg, L., Dirisu, A., Hurst, D., Hall, E., Jordan, A., and Vömel, H.: Correction technique for Raman water vapor lidar signal-dependent bias and suitability for water vapor trend monitoring in the upper troposphere, Atmos. Meas. Tech., 5, 2893-2916, https://doi.org/10.5194/amt-5-2893-2012, 2012.

Wulfmeyer, V., H. Bauer, M. Grzeschik, A. Behrendt, F. Vandenberghe, E.V. Browell, S. Ismail, and R.A. Ferrare: Four-Dimensional Variational Assimilation of Water Vapor Differential Absorption Lidar Data: The First Case Study within IHOP_2002, Mon. Wea. Rev., 134, 209–230, https://doi.org/10.1175/MWR3070.1, 2006.

Wulfmeyer, V., R. M. Hardesty, D. D. Turner, A. Behrendt, M. P. Cadeddu, P. Di Girolamo, P. Schlüssel, J. Van Baelen, and F. Zus: A review of the remote sensing of lower tropospheric thermodynamic profiles and its indispensable role for the understanding and the simulation of water and energy cycles, Rev. Geophys., 53, 819–895, doi:10.1002/2014RG000476, 2015.

Yoshida, S., T. Sakai, T. Nagai, S. Yokota, H. Seko, Y. Shoji: Feasibility study of data assimilation using a mobile water vapor Raman lidar, Proceedings of the 19th conference on coherent laser radar technology and applications, 251-255, https://clrccires.colorado.edu/data/paper/P21.pdf, 2018a.

Yoshida, S., T. Sakai, T. Nagai, S. Yokota, H. Seko, and Y. Shoji: Data assimilation of water vapor mixing ratio observed by a lidar to forecast heavy precipitation, J. Meteor. Soc. Japan, (to be submitted), 2018b.